ORIGINAL PAPER

Peak Shear Strength of Natural, Unfilled Rock Joints in the Field Based on Data from Drill Cores – A Conceptual Study Based on Large Laboratory Shear Tests

F. Ríos-Bayona[1] · F. Johansson[1] · J. Larsson[1,2] · D. Mas-Ivars[1,3]

Abstract

Significant uncertainties remain regarding the field assessment of the peak shear strength of rock joints. These uncertainties mainly originate from the lack of a verified methodology that would permit prediction of rock joints' peak shear strength accounting for their surface area, while using information available from smaller samples. This paper investigates a methodology that uses objective observations of the 3D roughness and joint aperture from drill cores to predict the peak shear strength of large natural, unfilled rock joints in the field. The presented methodology has been tested in the laboratory on two natural, unfilled rock joint samples of granite. The joint surface area of the tested samples was of approximately 500×300 mm. In this study, the drill cores utilised to predict the peak shear strength of the rock joint samples are simulated based on a subdivision of their digitised surfaces obtained through high-resolution laser scanning. The peak shear strength of the tested samples based on the digitised surfaces of the simulated drill cores is predicted by applying a peak shear strength criterion that accounts for 3D roughness, matedness, and specimen size. The results of the performed analysis and laboratory experiments show that data from the simulated drill cores contain the necessary information to predict the peak shear strength of the tested rock joint samples. The main benefit of this approach is that it may enable the prediction of the peak shear strength in the field under conditions of difficult access.

Highlights

- The peak shear strength of two large-size rock joint samples is predicted based on small-size drill cores simulated on their joint surfaces.
- The results obtained show that the simulated drill cores contain the necessary information to predict the peak shear strength of the tested samples.
- A sufficient number of simulated drill cores needs to be used to reduce the statistical uncertainty of the predicted values of peak shear strength.
- The rock joint aperture needs to be accounted for and measured directly in the borehole under the prevailing level of normal stress.
- The main benefit of this approach is that it may enable the prediction of the peak shear strength in the field under conditions of difficult access.

✉ F. Ríos-Bayona
  frrb@kth.se

  F. Johansson
  fredrik.johansson@byv.kth.se

  J. Larsson
  jorgen.larsson@ri.se

  D. Mas-Ivars
  diego.masivars@skb.se

[1] Division of Soil and Rock Mechanics, Department of Civil and Architectural Engineering, KTH Royal Institute of Technology, Brinellvägen 23, 100 44 Stockholm, Sweden

[2] Division of Material and Production, Department of Chemistry and Applied Mechanics, RISE Research Institutes of Sweden, Borås, Sweden

[3] SKB Swedish Nuclear Fuel and Waste Management Co, Solna, Sweden

Abbreviations

2D-DIC	2D Digital Image Correlation
CNL	Constant normal load
DC	Drill core simulated on the digitised rock joint surface
ISRM	International Society for Rock Mechanics
JCS	Joint wall compressive strength
JRC	Joint roughness coefficient
KTH	Royal Institute of Technology, Sweden
LVDT	Linear variable differential transformer
NWMO	Nuclear Waste Management Organization of Canada
RISE	Research Institutes of Sweden
SKB	Swedish Nuclear Fuel and Waste Management Co

Roman letters

a_{50}	Measured rock joint median aperture
a_{mean}	Measured rock joint mean aperture
a^*	Amplitude constant based on asperity base length
A	Area of the rock joint sample
A_0	Maximum potential contact area ratio
A_c	Total contact area
$A_{c,p}$	Potential contact area ratio
A_S	Area at small size
C	Roughness parameter
F_n	Normal force
h_{asp}	Asperity height
H	Hurst exponent
i	Incremental dilation angle measured in direct shear test
i_g	Dilation angle at grain size
i_n	Dilation angle at sample size
i_p	Dilation angle at measured peak shear strength
k	Matedness constant
L_{asp}	Asperity base length
$L_{asp,g}$	Average length of the asperities in contact at size associated with grain size
L_g	Length of the asperities associated with grain size
L_n	Length of the rock joint sample at large size
$\boldsymbol{n}$	Normal vector to the digitised joint surface
N_{DC}	Number of drill cores used to predict the peak shear strength
N_x, N_y	Coordinate points over a digitised joint surface parallel and perpendicular to shear direction
R^2	Coefficient of determination
$\boldsymbol{t}$	Vector against the shear direction
T	Shear force
$T_{p,L}$	Peak shear force at large size
$T_{p,S}$	Peak shear force at small size
Z_2	Root mean square of the first derivate of the joint surface

Greek letters

δ_n	Normal displacement
δ_s	Shear displacement
$\delta_{s,p}$	Shear displacement at measured peak shear strength
$\Delta x, \Delta y$	Sampling distance parallel and perpendicular to the shear direction
θ^*	Apparent dip angle
θ^*_{max}	Maximum apparent dip angle
μ	Mean value
σ	Standard deviation
σ_{ci}	Uniaxial compressive strength of the joint surface
σ_μ	Standard deviation of the mean value
σ_n	Normal stress
$\tau_{p,L}$	Peak shear stress at large size
$\tau_{p,S}$	Peak shear stress at small size
ϕ	Mobilised friction angle
ϕ_b	Basic friction angle
ϕ_p	Peak friction angle

1 Introduction

The rock joint shear strength at field scale is an important design parameter and remains a challenge for rock mechanics engineers. In recent decades, researchers have studied the influence of joint surface area on the mechanical behaviour of rock joints. The findings from the performed experiments are various and indicate that the mechanism behind the widely accepted scale effect is not yet completely understood. For instance, various studies on the shear behaviour of rock joints show that their peak shear strength decreases when the size of the tested specimens increases (Pratt et al. 1974; Barton and Choubey 1977; Bandis 1980; Bandis et al. 1981; Muralha and Pinto Da Cunha 1990; Yoshinaka et al. 1993; Ohnishi and Yoshinaka 1995; Huang et al. 2020a). This is commonly referred to as a negative scale effect. In an attempt to reproduce the experiment conducted by Bandis (1980) on the influence of specimen size on the shear behaviour of rock joints, Hencher et al. (1993) also observed that the measured peak shear strength was, on average, higher for the smaller samples. However, Hencher et al. (1993) observed that the effect of specimen size on the shear behaviour of the tested samples disappeared after correction for dilation of the shear stress vs. shear displacement curves. Kutter and Otto (1990) observed both negative and positive scale effects (i.e., increasing peak shear strength with increasing specimen size) when testing rock joints with both

poor and perfect match between their joint surfaces, respectively. Both negative and positive scale effects have also been observed in tilt tests performed on two different rock types (Giani et al. 1995), and in direct shear tests performed at different levels of applied normal stress (Castelli et al. 2001). Other studies have reported the absence of a scale effect in the performed experiments (Johansson 2016), while some studies suggest that the utilised sampling method may influence the conclusions reached regarding the scale effect (Yong et al. 2019; Huang et al. 2020b).

According to the ISRM Suggested Method, the best way to account for the influence of joint surface area on the shear behaviour of natural rock joints is by conducting a direct shear test in-situ (Muralha et al. 2014). The performance of a direct shear test in-situ is, nevertheless, a complex procedure, due mainly to the difficulty of finding fully accessible joint surfaces at appropriate sizes (Barla et al. 2011). In rock engineering practice, the peak shear strength of large natural, unfilled rock joints in the field is often predicted based on information available at a smaller size, coming from visible traces or drill cores. However, there is not yet consensus regarding the most appropriate method to account for the influence of rock joint surface area when predicting peak shear strength based on information from field observations at a smaller size.

Barton and Bandis (1982) suggested that the influence of joint surface area on the peak shear strength of rock joints may be accounted for by reducing the parameters *JRC* and *JCS* with increasing size based on an empirical relationship. This empirical relationship mainly originates from the laboratory direct shear tests performed by Bandis (1980) on rock joint replicas with specimen size between 5 and 40 cm. However, as shown in Johansson (2016), the application of Barton and Bandis' empirical reduction to predict the peak shear strength of perfectly mated rock joints with different size can deviate from the observations in the direct shear tests made in the laboratory. Renaud et al. (2021) also observed that perfectly mated concrete-rock interfaces with different surface areas had a similar peak shear strength. Furthermore, Johansson (2016) concluded that the reported scale effects may be caused by the combination of not only the analysed rock joints' surface areas, but also the joint surfaces' matedness, as suggested by Zhao (1997a, b).

More recently, Casagrande et al. (2018) presented a semi-analytical stochastic approach that can predict both peak and residual shear strength of rock joints using the available information in 2D. Furthermore, Casagrande and colleagues believe their approach could potentially reduce the uncertainties associated with the scale effect, since it can be directly applied at the actual size of the problem (Casagrande et al. 2018; Buzzi and Casagrande 2018). However, a major limitation with the criterion from Casagrande et al. (2018) is that rock joint surfaces are assumed to be perfectly mated. In the field, the contact surfaces of natural, unfilled rock joints may exhibit a mismatch due to geological origin and deformation history (Odling 1994; Lanaro 2000), which results in a reduced peak shear strength not captured by the criterion (Ríos-Bayona et al. 2021a).

The above review shows that a methodology to predict the peak shear strength of large natural, unfilled rock joints in the field, based on information that can be observed at smaller sizes, is still lacking. Taking up this challenge, this paper presents a novel methodology that uses objective observations of 3D roughness and surface aperture from drill cores to predict the peak shear strength of large natural, unfilled rock joints in the field. The presented methodology has been tested in the laboratory on two rock joint samples with a surface area of approximately 500×300 mm. The rock joint samples were obtained from existing rock joints in the foundation of the Krångede concrete dam in Sweden. In this study, the peak shear strength of the samples tested in the laboratory is predicted based on observations of the roughness characteristics and surface aperture obtained from simulated drill cores. The simulated drill cores on the tested samples are based on a subdivision of their digitised joint surfaces obtained through high-resolution laser scanning. The predicted values of peak shear strength of the tested rock joint samples, based on the simulated drill cores of their digitised joint surfaces, are obtained by applying the peak shear strength criterion by Ríos-Bayona et al. (2021b). The criterion by Ríos-Bayona et al. (2021b) can account for the contribution of 3D surface roughness, matedness, and sample size when predicting the peak shear strength of natural, unfilled rock joints, an ability other failure criteria lack. The matedness of natural, unfilled rock joints is accounted for using the aperture measured between the joint surfaces obtained from the high-resolution laser scanning (Ríos-Bayona et al. 2021b).

2 Methodology

The hypothesis of the study presented in this paper is that it is possible to predict the peak shear strength of a large natural, unfilled rock joint in the field using information obtained from a number of representative drill cores. To investigate the validity of this hypothesis, analytical and experimental work was performed on two rock joint samples of coarse-grained granite. The main steps described in this section are illustrated in the flow chart in Fig. 1.

The dimension of the two rock joint samples analysed in this study was approximately $500 \times 300 \times 350$ mm ($L \times W \times H$). The rock joint samples were saw-cut from existing rock joints in the foundation of a concrete dam. For each sample, high-resolution laser scanning of the natural joint surfaces was performed prior to the direct shear tests.
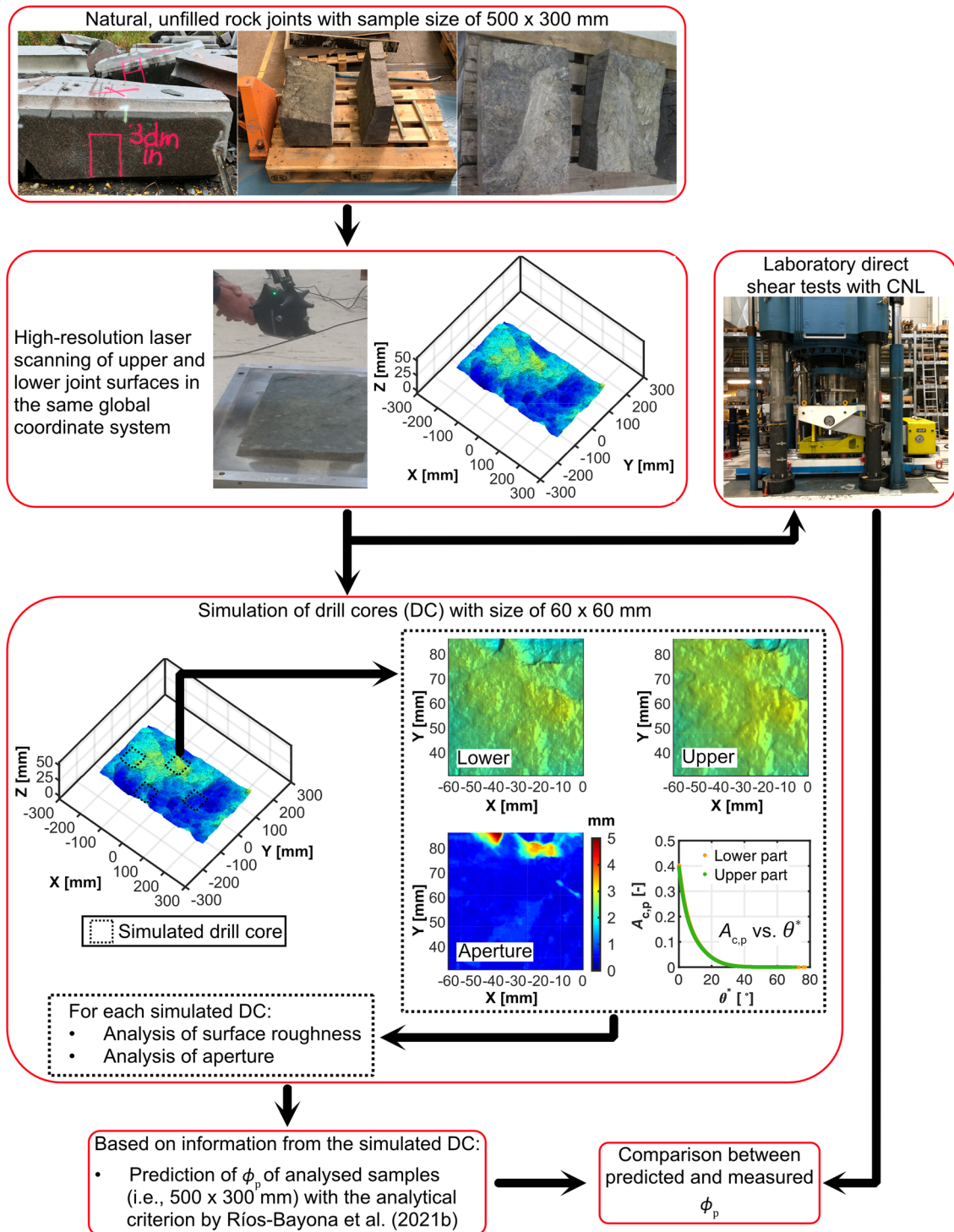
Fig. 1 Flow chart with the main steps followed to investigate the validity of the hypothesis that information from 3D surface roughness and aperture at small size can be used to predict the peak shear strength of a large natural, unfilled rock joint in the field

Both the lower and upper parts were scanned in the same global coordinate system to capture the degree of contact between the joint surfaces. The superposition of the scanned surfaces in the same global coordinate system allowed for

the analysis of the joint aperture, as in Ríos-Bayona et al. (2021b). The digitised joint surfaces were subdivided into smaller surfaces with a size of approximately 60×60 mm. The idea with each of these smaller-size surfaces was to

simulate a drill core (DC) obtained after borehole drilling the larger rock joint samples under study in the laboratory. For each simulated DC, both the aperture and surface roughness were analysed using only the information contained in the scanning of each defined surface at small size, as illustrated in Fig. 1. The surface roughness of each simulated DC was measured using the three roughness parameters proposed by Grasselli (2001), and self-affine fractal theory (Mandelbrot 1985; Renard et al. 2006; Stigsson and Mas Ivars 2019). The three roughness parameters by Grasselli (2001) are the maximum possible contact area ratio (A_0), the maximum apparent dip angle of the asperities in the shearing direction (θ^*_{max}), and the roughness parameter (C). The idealisation of surface roughness based on the principles of self-affine fractal theory as a superposition of different asperities at multiples scales is expressed in terms of the amplitude constant (a^*) and the Hurst exponent (H). The values of peak shear strength based on the simulated DC in the digitised surfaces of the tested samples were obtained by applying the peak shear strength criterion by Ríos-Bayona et al. (2021b). The formulation of the peak shear strength criterion and the theory applied in this study to predict the peak shear strength based on DC are further explained in Sect. 3.

The predicted values of peak friction angle (ϕ_p) based on simulated DC were compared with the ϕ_p measured in the laboratory direct shear tests of rock joint samples with surface area of 500 × 300 mm under constant normal load (CNL) conditions. Based on the results from the comparison, the uncertainties associated with the prediction of ϕ_p of large natural, unfilled rock joints in the field are further discussed.

3 Theory

3.1 Rationale and Formulation of the Criterion by Ríos-Bayona et al. (2021b)

The peak shear strength criterion by Ríos-Bayona et al. (2021b) is a revised version of the peak shear strength criterion by Johansson and Stille (2014), further validated by Johansson (2016). The criterion is based on the adhesion theory of friction, first stated by Terzhagi (1925) and later shown by Bowden and Tabor (1950a, b) to be able to explain the frictional behaviour of a wide range of materials, and it assumes that sliding is the governing failure mode along the active asperities in contact (Johansson and Stille 2014). Furthermore, the criterion accounts for the contribution from 3D surface roughness, matedness and sample size when predicting the peak shear strength of natural, unfilled rock joints. The matedness of natural, unfilled rock joints is estimated using objective measurements of the aperture

between their contact surfaces. This is done by a theoretical association between the joint surface aperture and the size and inclination of the active asperities in contact that contribute to the peak shear strength. The theoretical association between aperture and inclination of the active asperities is based on the assumption that the surface roughness can be described using self-affine fractal theory (Mandelbrot 1985; Renard et al. 2006; Stigsson and Mas Ivars 2019). The peak shear strength criterion has been validated with results from direct shear tests performed in the laboratory on rock joint samples with sizes up to 240 × 240 mm and different surface matedness (Johansson and Stille 2014; Johansson 2016; Ríos-Bayona et al. 2021b).

The criterion can be expressed as

$$\phi_p = \phi_b + i_n, \tag{1}$$

in which

$$i_n = \arctan\left[\tan(i_g)\left(\frac{L_n}{L_g}\right)^{k(H-1)}\right], \tag{2}$$

and

$$i_g = \theta^*_{max} - 10^{\left(\frac{\log_{10}\frac{\sigma_n}{\sigma_{ci}} - \log_{10}A_0}{C}\right)}\theta^*_{max}, \tag{3}$$

where ϕ_b is the basic friction angle for a dry and sawn surface, i_n and i_g are the dilation angle at sample and grain sizes, respectively, L_n is the length of the sample, L_g is the length of the asperities associated with grain size, k is the matedness constant, σ_n is the applied normal stress, and σ_{ci} is the uniaxial compressive strength of the joint surfaces.

The derivation of i_g in Eq. (3), which was first established by Johansson and Stille (2014), has recently been discussed by Li (2021) and Du et al. (2021). As a clarification, Eq. (3) is valid for ratios of actual contact areas facing the shear direction (A_c) to the total area of the joint surface (A) that range from 0 to A_0. The parameter A_0 is normally around 0.5 (Grasselli 2001; Grasselli et al. 2002). Furthermore, the derivation of Eq. (3) is based on a theoretical association between the ratios A_c/A and σ_n/σ_{ci} based on the adhesion theory, as well as that sliding is the governing failure mode along the active asperities in contact (Johansson and Stille 2014). The formulation presented in Li (2021) wrongly assumes that, for rough rock joints, the ratio A_c/A can vary within the range of 0 to 1. The equation derived by Li (2021) introduces a discrepancy between the actual inclination of the asperities in contact and the calculated inclination using his formula. This should be avoided. Additionally, as observed by Grasselli and Egger (2003), dilation due to sliding is entirely replaced by shearing at sufficiently high ratios of σ_n/σ_{ci}, or A_c/A, within the range of 0.15 and 0.2 (Du et al. 2021).
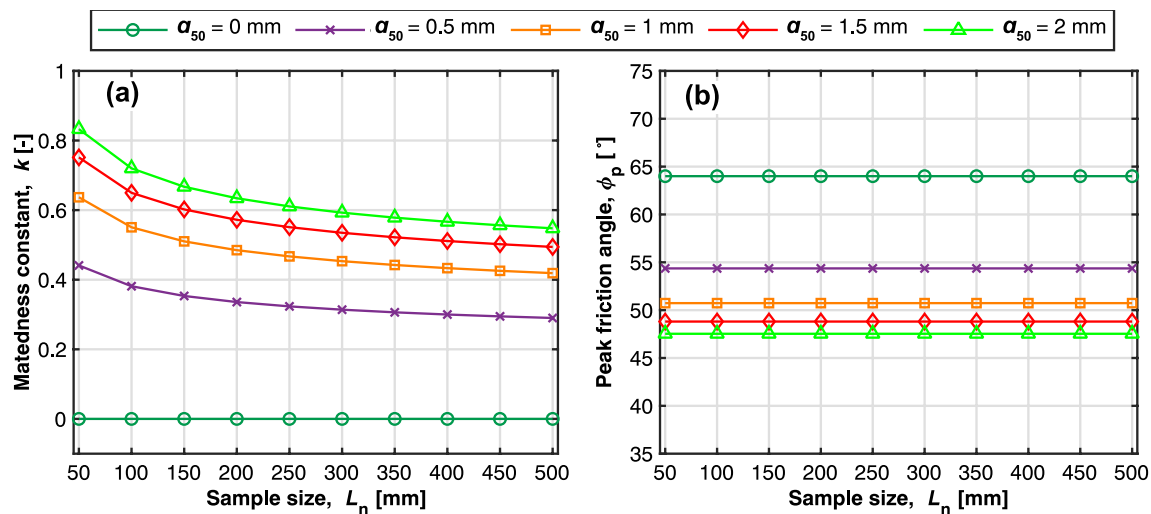
Fig. 2 Influence of a_{50} on the parameter k (**a**) and on the predicted ϕ_p (**b**) for different values of L_n using Eqs. (1) to (4), assuming a $\phi_b = 29°$, $\sigma_n = 1$ MPa, $i_g = 35°$, and $H = 0.8$

The equation for k is given by

$$k = \frac{\log_{10}\frac{2 \cdot a_{50}}{\tan(i_n)} - \log_{10}L_{asp,g}/2}{\log_{10}L_n/2 - \log_{10}L_g/2},\tag{4}$$

where a_{50} is the measured median aperture between the rock joint surfaces at the beginning of the shearing process, and $L_{asp,g}$ is the average length of the asperities in contact at grain size.

The parameter k in Eq. (4) directly associates a_{50} with both L_n and i_n (i.e., the inclination of the active asperities in contact that contribute to the peak shear strength). This theoretical association between a_{50}, L_n and i_n is based on the principles of self-affine fractal theory and that sliding is the predominant failure mode along the active asperities (Johansson and Stille 2014; Johansson 2016; Ríos-Bayona et al. 2021b).

The incorporation of a_{50} in the calculation of k in Eq. (4) is a modification of the original version presented in Ríos-Bayona et al. (2021b), which uses the measured mean aperture (a_{mean}). Due to the possibility of having an asymmetric distribution of the measured aperture, a more accurate assumption is to use the value of a_{50} instead of a_{mean}. Therefore, the value of k can vary between 0 for a perfectly mated rock joint (i.e., $a_{50} = 0$) and 1 for a totally mismatched rock joint (i.e., maximum possible a_{50} due to dilation originating from sliding along the active asperities).

The criterion by Ríos-Bayona et al. (2021b) uses the digitised joint surfaces to objectively measure the roughness characteristics and the value of a_{50}, and estimates the values of i_g, i_n and k by performing an iterative process with

Eqs. (2), (3), and (4). The predicted ϕ_p is obtained with Eq. (1).

3.2 Interaction Between Roughness and Aperture at Different Sample Sizes

In the criterion by Ríos-Bayona et al. (2021b), the peak shear strength is regarded as the result of a mean value-driven process to which each asperity in contact during the shearing process contributes. Furthermore, the criterion assumes that it is the size and inclination of these active asperities in contact that determines the peak shear strength, rather than the total size of the tested samples. As shown by Eqs. (2) to (4), the size and inclination of the active asperities in contact are directly influenced by the measured aperture between the contact surfaces. This means that, under the same applied σ_n magnitude, the predicted value of ϕ_p with the criterion for rock joint samples of different sizes remains constant, given that their measured values of both surface roughness (i.e., A_0, θ^*_{max}, C, and H) and surface aperture (i.e., a_{50}) are the same. As an example, the evolution of the parameter k and the predicted ϕ_p with the criterion [Eqs. (1) to (4)] at different values of both L_n and a_{50} is illustrated in Fig. 2. The calculations were performed with a $\phi_b = 29°$, $\sigma_n = 1$ MPa, and assuming same values of $i_g = 35°$, and $H = 0.8$.

The results illustrated in Fig. 2 show that, for the same value of a_{50}, the parameter k obtained from the iterative process with Eqs. (2) to (4) decreases with increasing L_n. However, the size and inclination of the active asperities in contact remain unchanged at different L_n. This is mainly because the theoretical association between the size and inclination of the active asperities in contact in the criterion is governed by a_{50}. This theoretical assumption is connected

Fig. 3 **a** Concrete dam at Krångede; **b** large rock blocks obtained by wire-cutting and lifted up during the excavation of the vertical shafts (the marks in magenta colour indicate the dimensions for laboratory sample cutting); **c** rock joint sample K1 before encapsulation in the specimen holder; **d** rock joint sample K2 before encapsulation in the specimen holder

to the possibility of describing surface roughness using self-affine fractal theory, which means that the roughness can be considered as a superposition of different asperities at multiple scales (Mandelbrot 1985; Renard et al. 2006; Stigsson and Mas Ivars 2019). For instance, this assumption shall not be applied to predict the peak shear strength of blasted joint surfaces or saw-tooth rock joints. Consequently, the predicted value of ϕ_p is constant and independent of L_n if the joint surfaces have same values of A_0, θ^*_{max}, C, H, and a_{50}. This is logical since according to the criterion it is the number, size, and inclination of the contact asperities that mainly governs the peak shear strength (Johansson and Stille 2014; Johansson 2016; Ríos-Bayona et al. 2021b).

3.3 Prediction of Peak Shear Strength of Large-Size Samples Based on Drill Cores

Based on the interaction between surface roughness and aperture shown in Fig. 2, it is reasonable to assume that $\tau_{p,L} = \tau_{p,S}$, where $\tau_{p,L}$ is the peak shear stress at large size, and $\tau_{p,S}$ is the peak shear stress at small size. In addition, the total peak shear force of a large sample ($T_{p,L}$) can be regarded as the sum of the peak shear forces of smaller samples, such as drill cores, given that they cover the entire joint surface area of the large sample. This can be expressed as $T_{p,L} = \sum_{i=1}^{n} T_{p,S_i}$, where n is the total number of drill cores over the complete surface, and T_{p,S_i} is the peak shear force from each individual drill core. By extension,

$T_{p,L} = \sum_{i=1}^{n} \tau_{p,S_i} \cdot A_{p,S_i}$. Furthermore, the peak shear strength can be regarded as a mean value-driven process, where each individual subarea can be seen as an independent component in a parallel system. Based on this assumption, $T_{p,L}$ can be calculated as the product of the mean value of the predicted peak shear stress ($\mu_{\tau_{p,S}}$) of the drill cores and the total area of the large sample (i.e., $T_{p,L} = \mu_{\tau_{p,S}} \cdot A$). Therefore, for a large rock joint sample, the peak shear strength can be derived as the mean value of the predicted peak shear strength of several drill cores of smaller size, based on both the applied magnitude of σ_n, and the measured values of ϕ_b, σ_{ci} A_0, θ^*_{max}, C, H, and a_{50}.

4 Rock Joint Samples

The analysed rock joint samples were obtained from two existing natural, unfilled rock joints adjacent to the foundation of the Krångede concrete dam in Sweden. The samples were saw-cut from two larger rock blocks coming from the excavation of new vertical shafts in connection with the existing power plant at Krångede. The vertical shafts were excavated using wire-cutting for safety reasons. Figure 3 illustrates the Krångede concrete dam, part of the large blocks lifted up from the vertical shafts, and the two saw-cut rock joint samples analysed in this study with dimensions of approximately $500 \times 300 \times 350$ mm (K1 and K2).

Table 1 Size, test conditions during the shear tests, and values of ϕ_b and σ_{ci} for the analysed rock joint samples from Krångede

Sample	L_n [mm][a]	Width [mm]	Area [cm²]	Test conditions	ϕ_b [°]	σ_{ci} [MPa]
K1	500.0	292.5	1462.5	CNL ($\sigma_n = 1$ Mpa)	29	150
K2	505.0	305.0	1540.3	CNL ($\sigma_n = 1$ Mpa)	29	150

[a]Measured in the shear direction

Based on observations from the large rock blocks in Fig. 3b, the rock mass beneath the dam's foundation consists of red coarse-grained granite of Proterozoic age (1.6–1.5 Ga), and contains a persistent sub-horizontal joint set. The joints in this joint set are believed to have been formed because of stress relief from denudation. As a result, the joints were induced from tensile stresses and have therefore rough surfaces without any exposure to previous shear displacements. The joint surfaces of K1 and K2 were slightly weathered and had thin coatings of chlorite and calcite (see Fig. 3c, d). The thickness of the observed coatings of calcite and chlorite was estimated to be approximately a tenth of a millimetre. The value of ϕ_b was estimated to be 29°, obtained by means of tilt tests on rectangular saw-cut specimens following the ISRM Suggested Method (Alejano et al. 2018). The tilt tests were performed on eight rectangular-based specimens saw-cut with dimensions of $80 \times 70 \times 20$ mm. The saw blade used to cut the samples had a diameter of 900 mm, a width of 5 mm, a grain size of 0.2 to 0.3 mm, and a diamond concentration of 50 pcs. The tilt tests were performed using a manually operated tilting platform. The utilised tilting platform had the capability of measuring tilting angles with a resolution of $\pm 0.5°$. During the tests, the allowed sliding distance was approximately 10% of the maximum length of the rectangular specimens. The tilting velocity was approximately 10°/min.

The value of ϕ_b (29°) derived in this study is consistent with other previous results reported in coarse-grained granite samples with fresh surfaces (Alejano et al. 2012; Johansson 2016). However, this ϕ_b value may be slightly overestimated due to the observed coatings on the actual rock joint surfaces of samples K1 and K2. For instance, other experiments have found that the dilation-corrected basic friction of natural joint surfaces with chlorite coating may be considerably lower than the measured ϕ_b obtained through planar, fresh surfaces (Hencher and Richards 2015). The uncertainty in the actual ϕ_b due to the presence of thin coatings of chlorite and calcite on the joint surfaces of samples K1 and K2 is further investigated in Sect. 7 based on the results of the laboratory direct shear tests.

The σ_{ci} of the joint surfaces of samples K1 and K2 was estimated to be 150 MPa using the Schmidt Hammer Index, according to the ISRM Suggested Method (Aydin 2008).

The dimensions of samples K1 and K2, conditions of the direct shear tests in the laboratory, and values of ϕ_b and σ_{ci} are shown in Table 1.

5 Rock Joint Surface Characterisation and Subdivision into Smaller Surfaces

5.1 Laser Scanning of the Joint Surfaces in 3D

The joint surfaces of samples K1 and K2 with dimensions of 500×300 mm were laser scanned before and after the direct shear tests. The measurements were performed using a Leica Absolute system manufactured by Hexagon, which consists of a laser tracker of type Leica AT960LR, in combination with a Leica T-probe mounted on a laser scanner of type Leica LAS. The scanner has a working range of ± 40 mm, a maximum sampling rate of 150,000 pts/s, and a minimum point density of 0.013 mm. The measurement accuracy of the scanner is ± 0.03 mm.

Samples K1 and K2 were scanned after the encapsulation process described in Sect. 6. The upper and lower joint surfaces of samples K1 and K2 were scanned separately, together with their respective specimen holders. The raw measurements of each part consisted of a point cloud with >100,000,000 coordinate points. Since the measurements were performed with the handheld scanner, the captured coordinate points were not initially organised in a regular mesh. The regular mesh utilised in the performed analysis of samples K1 and K2 was obtained by interpolation of the scanned points with a resolution (i.e., average nominal point spacing) of 0.2 mm. The utilised resolution was assumed appropriate to capture L_g of the rock joint samples, according to previous recommendations by Grasselli and Egger (2003) and Tatone and Grasselli (2009). The digitised joint surfaces of samples K1 and K2 in 3D, and with a resolution of 0.2 mm, are illustrated in Fig. 4.

Additionally, the upper and lower digitised joint surfaces were located in the same global coordinate system, using the 3D CAD model of the specimen holders as reference. This allowed for the analysis of the aperture between the joint surfaces of samples K1 and K2.
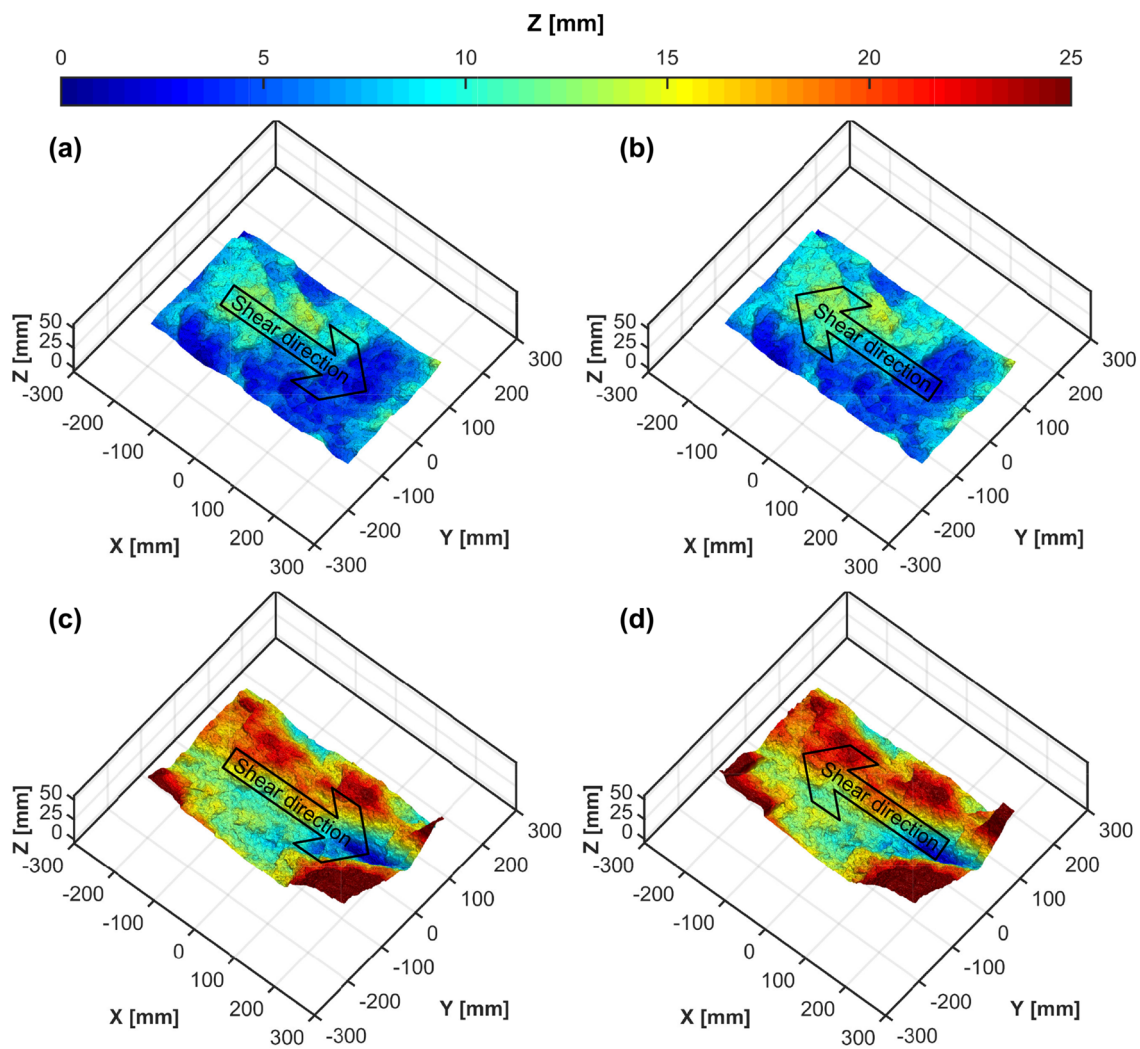
Fig. 4 Digitised joint surfaces of samples K1 and K2 with a resolution of 0.2 mm: **a** lower part of K1; **b** upper part of K1; **c** lower part of K2; **d** upper part of K2

5.2 Parameters for the Description of 3D Surface Roughness

Based on the digitised rock joint surfaces of samples K1 and K2 in Fig. 4, the roughness parameters (A_0, θ^*_{max} and C) of upper and lower parts were calculated using the following methodology: first, normal vectors ($\boldsymbol{n_i}$) were generated for each element in the mesh with a resolution of 0.2 mm. By defining the vector against the shear direction ($\boldsymbol{t}$), the values of apparent dip angle (θ^*) for each asperity were determined using

$$\cos\left(90° - \theta^*_i\right) = \frac{|\boldsymbol{n_i} \cdot \boldsymbol{t}|}{|\boldsymbol{n_i}| \cdot |\boldsymbol{t}|}. \tag{5}$$

This principle is illustrated in Fig. 5a. As an example, the calculated values of θ^* with respect to the defined $\boldsymbol{t}$ for the lower and upper parts of sample K1 are illustrated in Fig. 5b and c, respectively. Furthermore, for each value of θ^* calculated in the lower and upper parts of the analysed samples separately, the potential contact area ratio ($A_{c,p}$) was determined using the empirical relationship proposed by Grasselli (2001):

$$A_{c,p} = A_0 \left[\frac{\theta^*_{max} - \theta^*}{\theta^*_{max}}\right]^C. \tag{6}$$

The calculated values of $A_{c,p}$ versus θ^* for the lower and upper parts of sample K1 with a resolution of 0.2 mm are shown in Fig. 5d. The parameter C in Eq. (6) was calculated by nonlinear least-squares regression analysis as suggested by Tatone and Grasselli (2009). Table 2 presents the values of A_0, θ^*_{max}, and C for the upper and lower parts of samples K1 and K2.
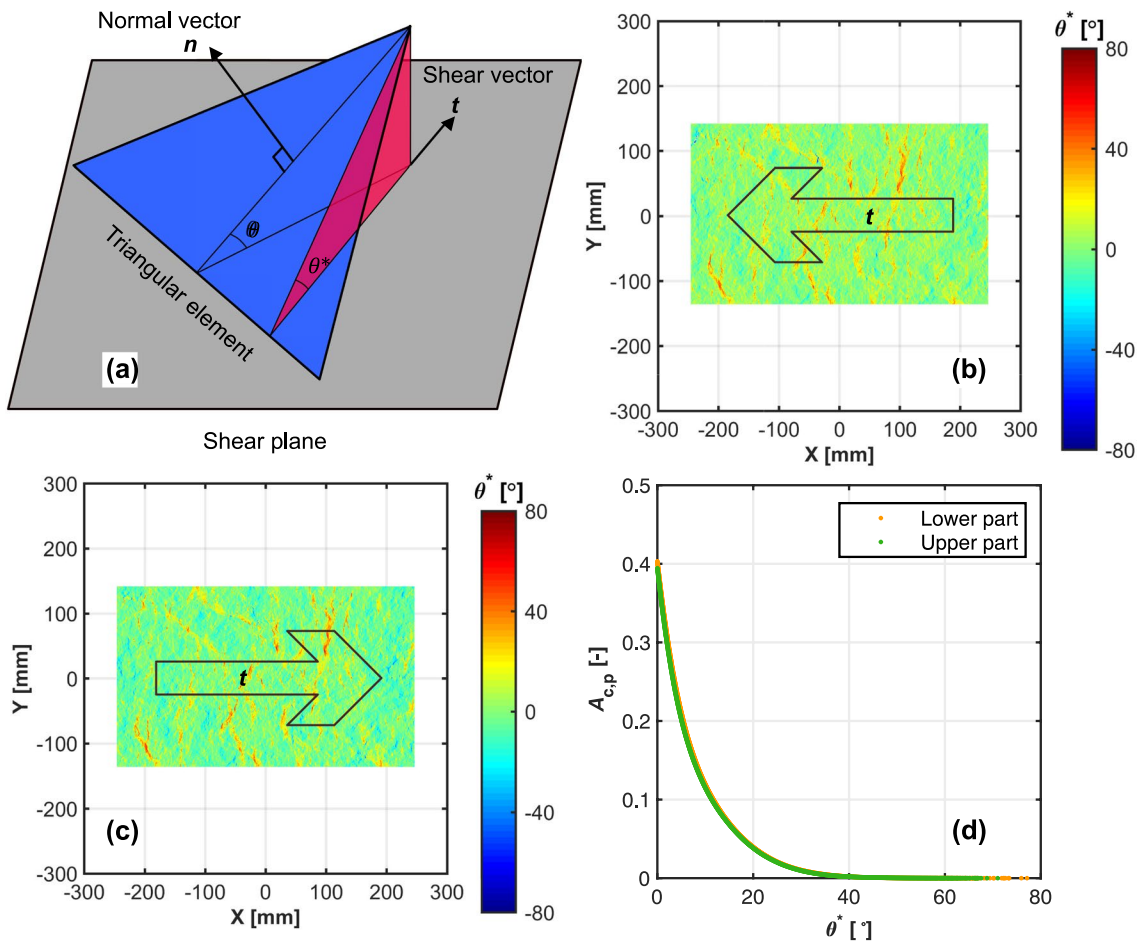
Fig. 5 **a** Illustration of the geometrical definition of θ^* of an asperity facing the defined t; **b** calculated values of θ^* in the lower part of sample K1 with respect to the defined t; **c** calculated values of θ^* in the upper part of sample K1 with respect to the defined t; **d** calculated values of $A_{c,p}$ vs. θ^* for the lower and upper parts of sample K1

Table 2 Values of A_0, $\theta^*_{\max}$, and C calculated for the lower and upper parts of samples K1 and K2

Sample	A_0 [–]	$\theta^*_{\max}$ [°]	C [–]	R^2 [–]
K1 lower part	0.403	77.1	8.74	0.997
K1 upper part	0.395	71.0	8.15	0.995
K2 lower part	0.501	82.2	9.40	0.997
K2 upper part	0.511	87.5	10.36	0.996

5.3 Description of Surface Roughness Based on Self-Affine Fractal Theory

The scaling relationship between the height of the asperities (h_{asp}) and their base length (L_{asp}), used when applying the criterion by Ríos-Bayona et al. (2021b), is based on the assumption that surface roughness can be described with self-affine fractal theory (Mandelbrot 1985; Renard et al. 2006; Stigsson and Mas Ivars 2019). Furthermore, a power

law relationship is also assumed between the variation of h_{asp} and the span of the measured profile (Brown 1987; Malinverno 1990; Johansson and Stille 2014). The power law relationship proposed by Johansson and Stille (2014) can be expressed as

$$h_{asp} = a^* L_{asp}^H. \tag{7}$$

To determine a^* and H, and to investigate the applicability of Eq. (7) to describe the scaling relationship between h_{asp} and L_{asp} in samples K1 and K2, the root mean square of the first derivative (Z_2) for different sampling intervals along the shear direction (Δx) in the digitised joint surfaces was calculated. The parameter Z_2 describes the average inclination of the asperities over a certain Δx and for each profile separated a sampling distance perpendicular to the shear direction (Δy). This can be expressed as
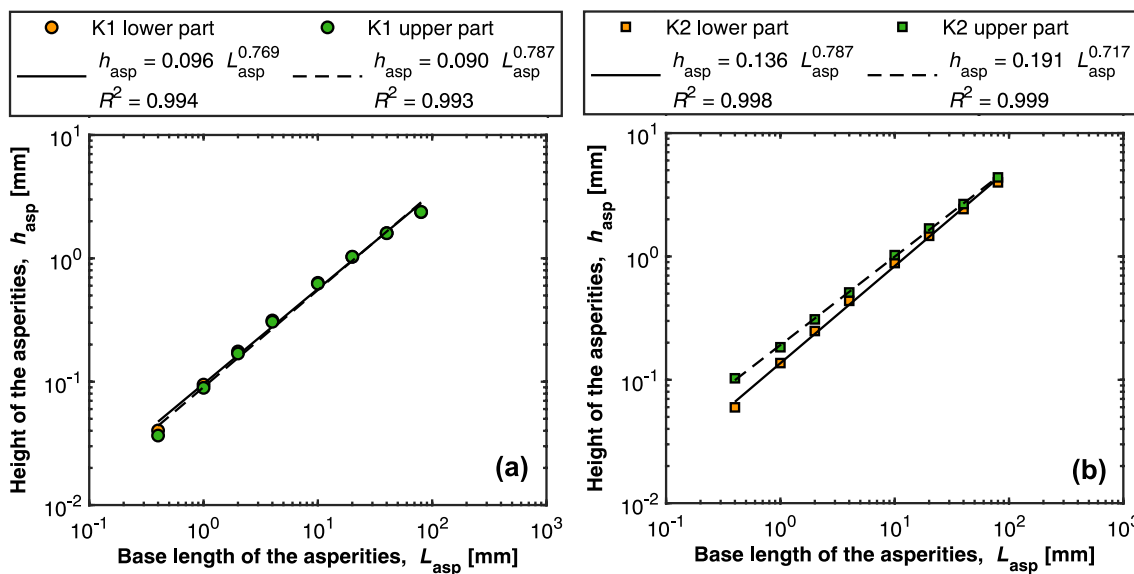
Fig. 6 Log–log plots with calculated values of h_{asp} for different values of L_{asp}, together with values of a^* and H calculated through linear regression using Eq. (7): **a** sample K1; **b** sample K2

$$Z_2 = \sqrt{\frac{1}{(N_x - 1) \cdot N_y} \sum_{j=1}^{N_y} \sum_{i=1}^{N_x-1} \left(\frac{z_{i+1,j} - z_{i,j}}{x_{i+1,j} - x_{i,j}} \right)^2}, \qquad (8)$$

where N_x and N_y are the number of coordinate points over a digitised rock joint surface parallel and perpendicular, respectively, to the shear direction. The pairs $(x_{i,j}, z_{i,j})$ and $(x_{i+1,j}, z_{i+1,j})$ are adjacent coordinates in the same profile along the shear direction separated by a constant distance Δx (Myers 1962).

The calculated values of h_{asp} for different values of L_{asp} using the digitised rock joint surfaces of samples K1 and K2, together with the values of a^* and H calculated through linear regression analysis using Eq. (7) are presented in Fig. 6. The values of Δx and Δy were equal and varied between 0.2 mm and 40 mm. Based on the results in Fig. 6, it can also be concluded that the surface roughness for both of the samples follows the power-law relationship in Eq. (7).

5.4 Analysis of Aperture Between the Joint Surfaces

The apertures of samples K1 and K2 were measured after superposing the lower and upper digitised surfaces with a resolution of 0.2 mm and calculating the difference in the vertical direction of all points with same x- and y-coordinates (i.e., $z_{i,j}^{upper} - z_{i,j}^{lower}$). Figure 7a, b show the aperture measurements of samples K1 and K2, respectively, oriented in the same global coordinate system. Samples K1 and K2 had a maximum

measured aperture of 8.3 and 29.4 mm, respectively. Figure 7c, d show the histograms of aperture of samples K1 and K2 with calculated values of a_{50} and a_{mean}, respectively. For each sample, a_{50} was obtained as the middle value of the measured aperture sorted in ascending order. The value of a_{mean} was obtained as suggested by Ríos-Bayona et al. (2021b):

$$a_{mean} = \frac{\sum_{i=1}^{N_x} \sum_{j=1}^{N_y} \left(z_{i,j}^{upper} - z_{i,j}^{lower} \right)}{N_x \cdot N_y}. \qquad (9)$$

The measured values of a_{50} and a_{mean} were 0.55 and 0.62 mm for sample K1, and 0.89 and 1.3 mm for sample K2, respectively.

5.5 Subdivision into Smaller-Size Surfaces Based on the Scanning Measurements

The digitised joint surfaces of samples K1 and K2 were subdivided into 40 smaller surfaces of approximately 60×60 mm. Each of the smaller-size surfaces simulated a DC obtained after borehole drilling the joint surfaces of samples K1 and K2.

The 3D surface roughness and aperture of each of the simulated DC in samples K1 and K2 were analysed following the same procedure as that applied at larger size to samples K1 and K2, described in Sects. 5.2, 5.3, and 5.4.
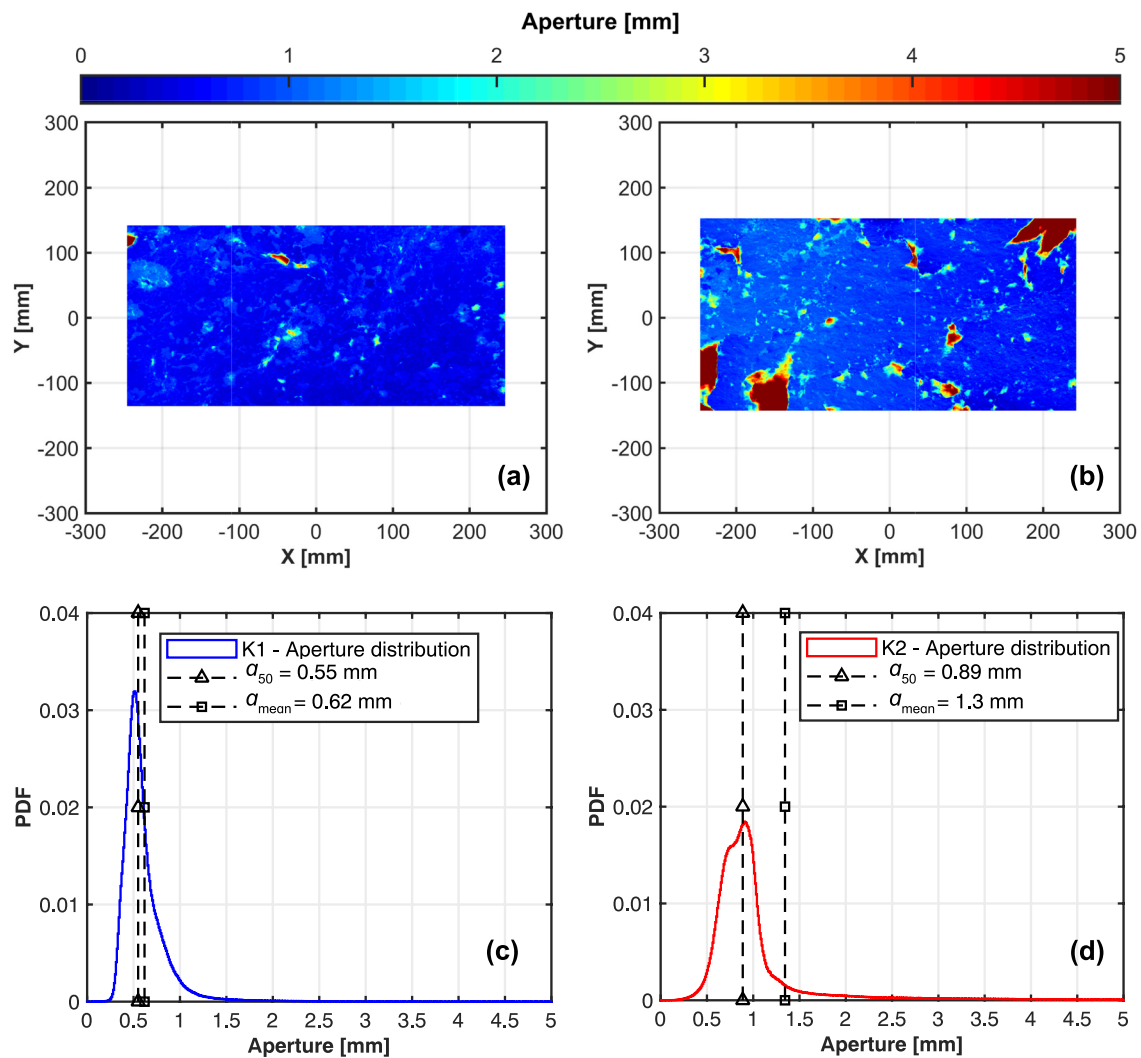
Fig. 7 Aperture measurements of samples K1 and K2 after superposing the lower and upper digitised surfaces: **a** difference between $z_{i,j}^{\mathrm{upper}}$ and $z_{i,j}^{\mathrm{lower}}$ of all coordinate points for sample K1; **b** difference between $z_{i,j}^{\mathrm{upper}}$ and $z_{i,j}^{\mathrm{lower}}$ of all coordinate points for sample K2; **c** histogram of aperture for sample K1; **d** histogram of aperture for sample K2

The procedure is illustrated in Fig. 8 for sample K1. Figures 9 and 10 show the values of A_0, $\theta_{\max}^*$, C, and H calculated for the upper and lower parts of the 40 DC simulated on samples K1 and K2, respectively. Figure 11 shows the values of a_{50} calculated after superposing upper and lower surfaces of the DC simulated on samples K1 and K2. The digitised upper and lower surfaces of the simulated DC with small size were in the same global coordinate system as the samples at large size. In some of the simulated DC, the superposition of the digitised upper and lower parts showed no contact between the joint surfaces, i.e., $\min\left(z_{i,j}^{\mathrm{upper}} - z_{i,j}^{\mathrm{lower}}\right) > 0$. This issue is further discussed in Sect. 8.

6 Laboratory Experimental Procedure

The rock joint samples K1 and K2 were sheared in a direct shear test equipment with the capacity to perform shear tests according to the ISRM Suggested Method (Muralha et al. 2014). This direct shear test equipment has been built mainly for use within the framework of the POST project. The POST project is a cooperative research programme involving SKB, NWMO, Posiva Oy (phase 1), RISE, and KTH that aims to increase understanding of rock fracture behaviour in nuclear waste repositories (Larsson 2021; Jacobsson et al. 2021).

The normal and shear capacity of this shear test equipment is 5 MN. The shear test equipment was mounted in a
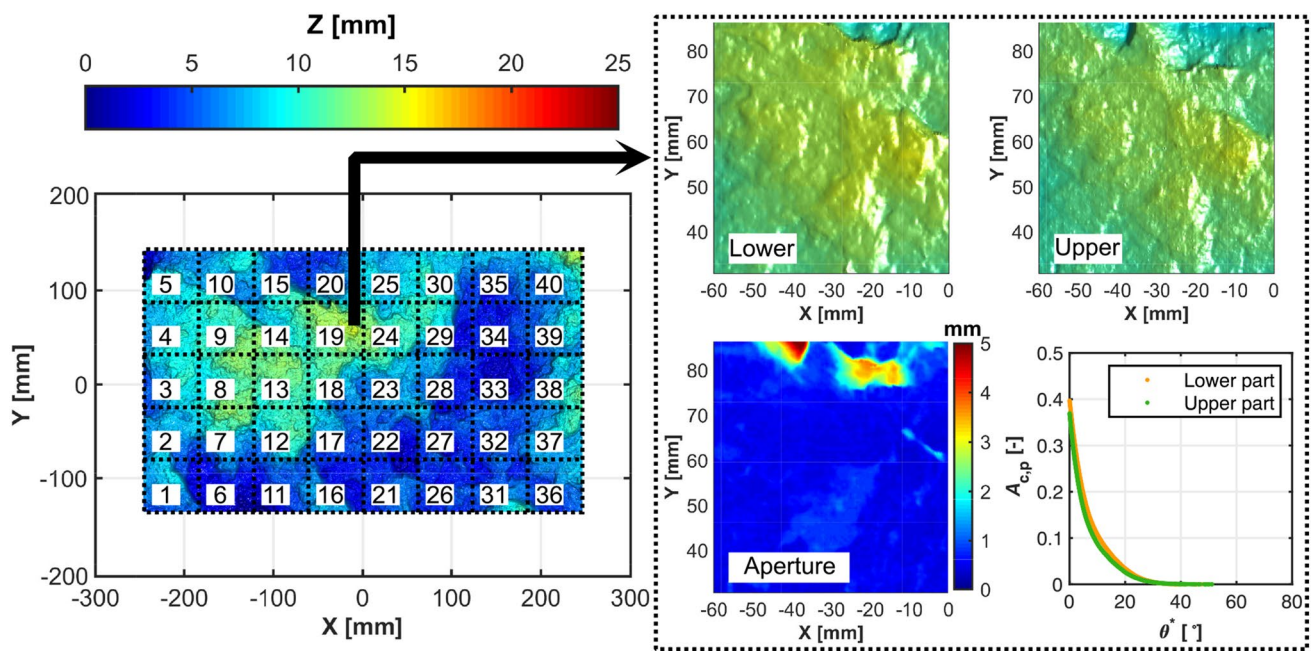
Fig. 8 Sample K1 subdivided in 40 surfaces of approximately 60×60 mm (left) and the analysis of the surface roughness and aperture of one of the simulated DC (right). Sample K2 was subdivided following the same procedure as for sample K1

loading frame, manufactured by MFL Systeme, with a normal loading capacity of 20 MN. Figure 12a shows the shear test equipment and the loading frame. The shear force (T) was applied by a stand-alone servo-hydraulic unit operating at 700 bars. In the shear direction, a force transducer of model type SW80M-5000kN-B383 from Tovey Engineering Inc. was used. The normal force (F_n) was applied by the built-in force transducer of the 20 MN loading frame. Data sampling and operation of the 5 MN shear test equipment and the 20 MN loading frame were executed from an MTS 100 control system.

The rock joint samples were fixed to the specimen holders with encapsulating high-strength grout of the type Ducorit® S5, manufactured by Densit. The concrete was mixed for 8–10 min with a water-to-cement (w/c) ratio of 0.068. The specimen holders were rectangular and made of 40 mm thick steel plates. The inside dimensions of each specimen holder were $650 \times 450 \times 190$ mm. The positioning between lower and upper parts of the specimen holders, and assembly into the shear test equipment, were done with a high-precision positioning system consisting of guide pins and guide plates. The vertical distance between upper and lower specimen holders in mounted position was 40 mm. Figure 12b, c illustrate the work performed during positioning and encapsulation of the lower part of sample K1 in the specimen holder.

Displacement transducers of model type ACT2000A, manufactured by RDP Electrosense, were used to measure both normal displacements (δ_n) (four locations) and shear displacements (δ_s) (two locations). The force and the displacement transducers were both calibrated and verified to have an uncertainty of less than 1%. During the tests conducted with sample K1, local measurements of δ_n and δ_s were additionally registered directly at the joint plane using 2D Digital Image Correlation (2D-DIC) measurements by Gom Correlate Professional. Four 5-megapixel machine vision cameras, of type Basler acA2440-20gm, were placed next to each of the vertical transducers in the vertical space between the specimen holders (40 mm). The cameras were equipped with 16 mm fixed focus length lenses from Edmund Optics. Figure 12d shows a detailed picture of the position of one installed vertical transducers and camera, prior to the direct shear test of sample K1. The camera configuration resulted in a field of view of 56×47 mm. The sampling rate of the DIC images was 1 frames/s. The values of F_n, T, δ_n and δ_s from the testing machine were simultaneously recorded in the DIC system. The local δ_n and δ_s along the joint plane were evaluated by DIC through a virtual strain gauge 10 mm in length, oriented in the normal loading direction symmetrically over the joint.

Prior to the direct shear tests, both samples K1 and K2 were subjected to a consolidating normal loading test. Four cycles were conducted with σ_n varying between 0.5 and 3 MPa applied at a loading rate of 1 MPa/min. The direct shear tests were conducted under CNL conditions with a σ_n
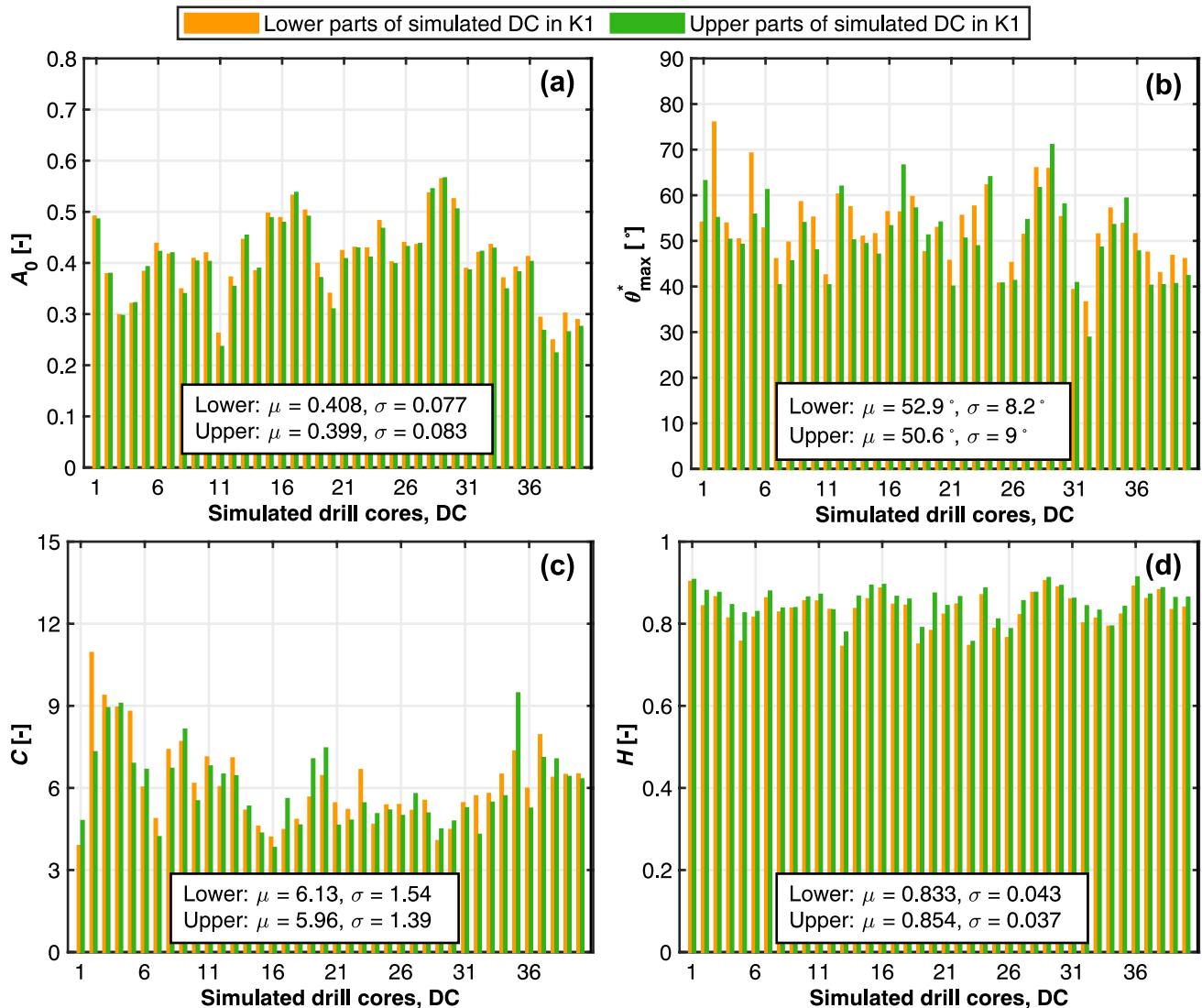
Fig. 9 Analysis of the surface roughness in the upper and lower parts of the 40 simulated DC in sample K1: **a** values of A_0; **b** values of θ^*_{max}; **c** values of C; **d** values of H. The values in the boxes indicate the mean value (μ) and standard deviation (σ) of each parameter in the lower and upper parts of the simulated DC, respectively

of 1 MPa. Shearing was carried out under a constant shear displacement rate of 0.2 mm/min until reaching a maximum δ_s of 50 mm. The data sampling rate during both the consolidating normal loading and direct shear tests was 10 Hz. The average values of δ_n and δ_s registered during the direct shear tests were used to calculate the incremental dilation angle (i) for each of the tested rock joint samples using

$$i = \arctan\left(\frac{d\delta_n}{d\delta_s}\right). \tag{10}$$

A constant $d\delta_s$ value of 0.1 mm was used in the calculation of i.

7 Shear Test Results and Peak Shear Strength Prediction

7.1 Shear Test Results

The results of σ_n versus δ_n, as measured during the consolidating normal loading tests, and the results of mobilised friction angle (ϕ) and δ_n versus δ_s, as measured during the direct shear tests conducted on samples K1 and K2, are presented in Fig. 13. Furthermore, the measured values of ϕ_p, dilation angle at the peak (i_p), and shear displacement at the peak ($\delta_{s,p}$) are presented in Table 3. The results of the direct shear tests containing ϕ versus δ_s are plotted mainly to maintain
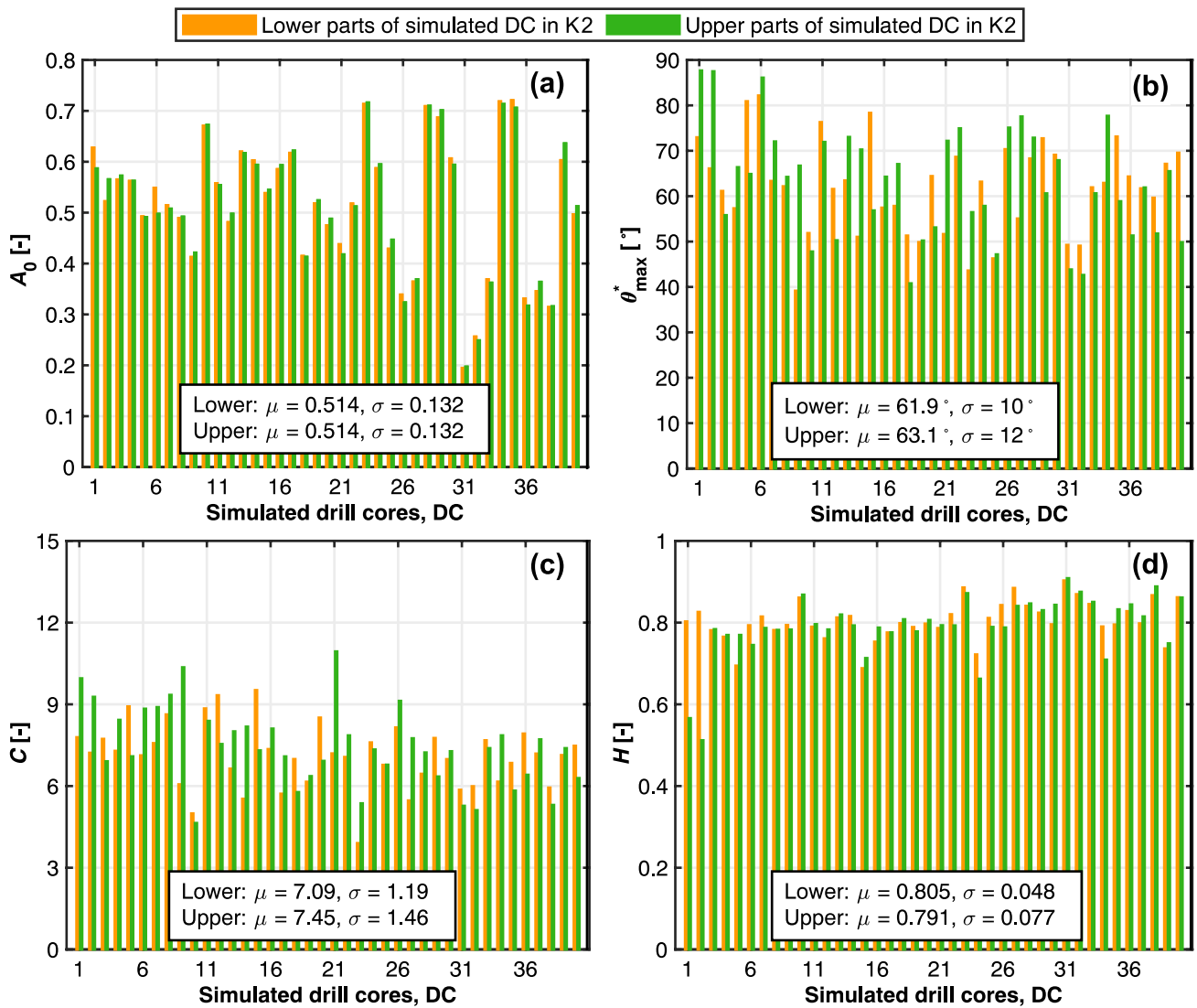
Fig. 10 Analysis of the surface roughness in the upper and lower parts of the 40 simulated DC in sample K2: **a** values of A_0; **b** values of θ^*_{max}; **c** values of C; **d** values of H. The values in the boxes indicate the μ and σ of each parameter in the lower and upper parts of the simulated DC, respectively

consistency in the comparison between the conducted shear tests and values of ϕ_p predicted with the criterion by Ríos-Bayona et al. (2021b).

Samples K1 and K2 showed similar mechanical behaviours during the consolidating normal loading tests (see Fig. 13a). On average, the measured δ_n, registered with the vertical LVDTs in the last three load cycles between a σ_n of 0.5 and 3 MPa, varied between 0.22 and 0.36 mm in sample K1, and 0.19 and 0.33 mm in sample K2. For the same interval of applied σ_n, the δ_n registered with the 2D-DIC measurements in sample K1 varied between 0.09 and 0.14 mm.

The results of the direct shear tests conducted on samples K1 and K2 also showed a similar mechanical behaviour, with a clear peak and post-peak behaviour (see Fig. 13b). Samples K1 and K2 showed a measured ϕ_p of 57.1° and 49.7°, respectively. The measured i_p was 20.3° and 17.8°, respectively. The registered values of $\delta_{s,p}$ were 0.98 mm in sample K1 and 0.71 mm in sample K2 (see Table 3). The measured values of residual ϕ at maximum δ_s were 39.3° in sample K1 and 42.3° in sample K2.

The comparison between measured δ_n versus δ_s in Fig. 13c showed a similar mechanical behaviour for samples K1 and K2, with a relative opening between their lower and upper parts from the beginning to the end of the direct shear tests. At a δ_s equal to 50 mm, the measured δ_n was 4.6 mm in sample K1, and 5.9 mm in sample K2. This observed mechanical behaviour in Fig. 13b, c indicates
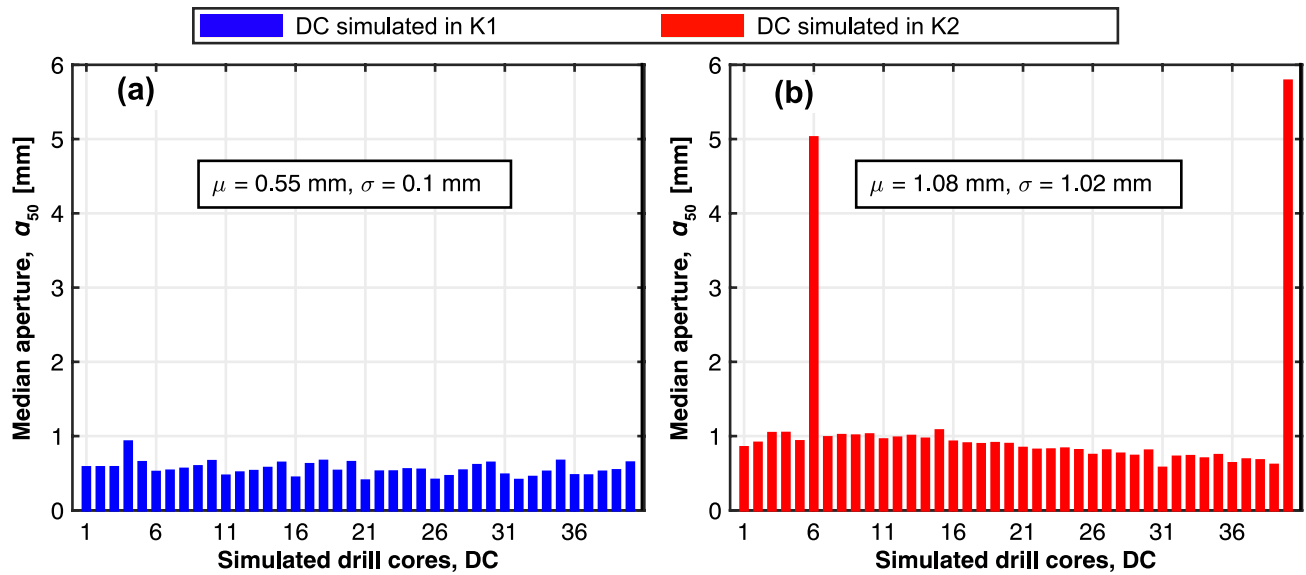
Fig. 11 Values of a_{50} calculated after superposing upper and lower surfaces of the 40 simulated DC on: **a** sample K1; **b** sample K2. The values in the boxes indicate the μ and σ of the a_{50}

Fig. 12 **a** Shear test equipment mounted in the loading frame at RISE; **b** lower part of sample K1 being placed into the specimen holder; **c** sample K1 after encapsulation of the lower part with high-strength grout Ducorite® S5; **d** detailed picture showing the position of one of the installed vertical transducers and camera prior the direct shear test of sample K1

that the thin coatings of calcite and chlorite in the contact points were worn away under the applied level of σ_n, thus allowing for rock-to-rock contact during the shearing process. This further means that, under the tested conditions, the influence of the thin coatings of chlorite and calcite on

the measured ϕ_p of samples K1 and K2 was most likely small and did not control the shear behaviour, as suggested by Barton and Choubey (1977). Additionally, the values of dilation-corrected friction at peak (i.e., $\phi_p - i_p$) derived from Table 3 were 36.8° for sample K1 and 31.9° for sample K2,
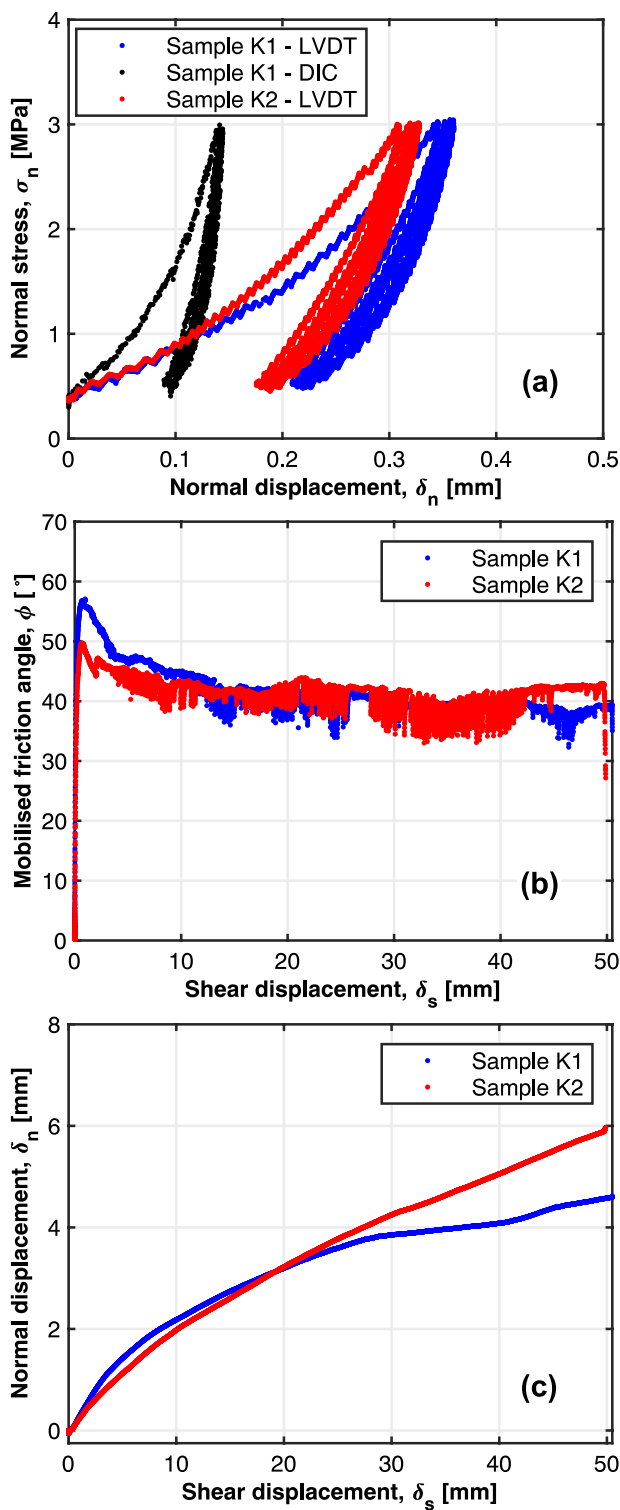
Fig. 13 Results of the consolidating normal loading and direct shear tests conducted in the laboratory on samples K1 and K2: **a** normal stress, σ_n vs. normal displacement, δ_n; **b** mobilised friction angle, ϕ vs. shear displacement, δ_s; **c** normal displacement, δ_n vs. shear displacement, δ_s

Table 3 Measured values of ϕ_p, i_p and, $\delta_{s,p}$ obtained in the laboratory direct shear tests conducted on samples K1 and K2

Sample	ϕ_p [°]	i_p [°]	$\delta_{s,p}$ [mm]
K1	57.1	20.3	0.98
K2	49.7	17.8	0.71

respectively. Both values are higher than the reported ϕ_b in Sect. 4, which is in agreement with values of dilation-corrected friction for granite previously reported (Hencher and Richards 2015). This further supports the conclusion that the influence from the observed chlorite coatings in samples K1 and K2 most likely is small.

7.2 Prediction of Peak Shear Strength Based on Simulated Drill Cores

To investigate the validity of the hypothesis presented in this study, the information regarding both 3D surface roughness and aperture, captured in each of the 40 simulated DC on samples K1 and K2, is used to predict their respective ϕ_p values. The use of simulated DC to predict the ϕ_p of samples K1 and K2 is based on the theory presented in Sect. 3.3. Therefore, the respective ϕ_p predicted for samples K1 and K2 is derived as the mean value of the predicted ϕ_p of the 40 simulated DC in their joint surfaces. The predicted values of ϕ_p of the simulated DC are obtained by applying the peak shear strength criterion by Ríos-Bayona et al. (2021b) presented in Sect. 3.1.

The values of predicted ϕ_p for the 40 DC simulated on the digitised joint surfaces of samples K1 and K2 are presented in Fig. 14a, b, respectively. The utilised values of A_0, θ^*_{max}, C, and H calculated for the lower and upper parts of the simulated DC on samples K1 and K2 are provided in Figs. 9 and 10, respectively. The values of a_{50} measured between the upper and lower parts of each simulated DC are provided in Fig. 11. The values of ϕ_b and σ_{ci} are provided in Table 1. The value of L_n used to predict the ϕ_p of all the simulated DC was 60 mm. The values of predicted ϕ_p for the 40 simulated DC on sample K1 vary between 42.6° and 70.3° (see Fig. 14a). The μ and σ of the predicted ϕ_p of the simulated DC on sample K1 are 51.8° and 6.5°, respectively. The predicted values of ϕ_p for the 40 simulated DC on sample K2 vary between 38.1° and 67.1° (see Fig. 14b). The μ and σ of the predicted ϕ_p of the simulated DC on sample K2 are 47.4° and 6.9°, respectively.

A comparison between the respective μ of the predicted ϕ_p based on the DC simulated on samples K1 and K2, and the predicted ϕ_p using their complete surfaces at large size, are presented in Fig. 14c. The input data necessary to predict the ϕ_p of samples K1 and K2 using their complete surfaces is provided in Tables 1, 2, and Figs. 6, 7c, d. The μ of predicted
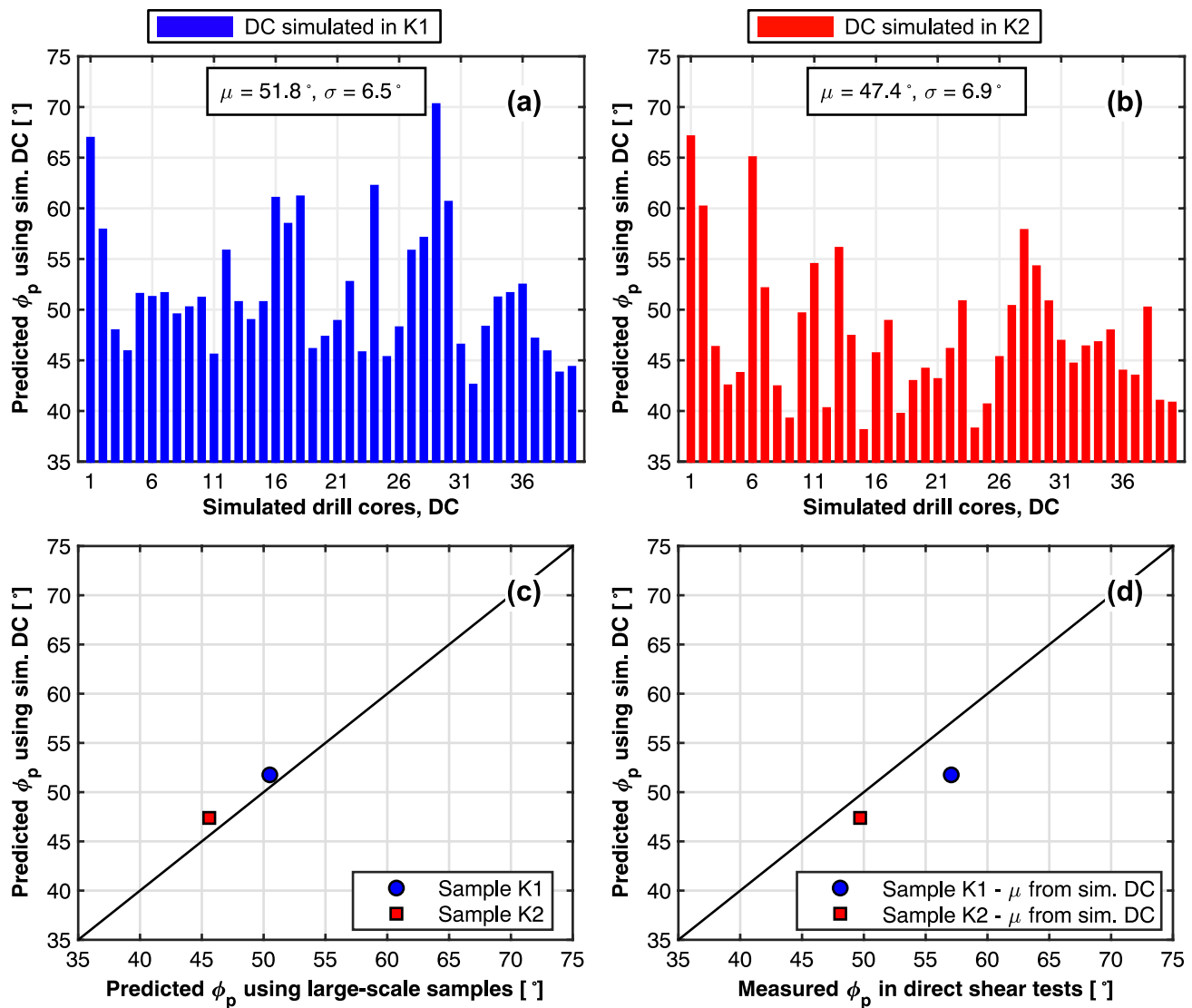
Fig. 14 **a** Predicted values of ϕ_p for the 40 DC simulated on the digitised surfaces of sample K1 using the criterion by Ríos-Bayona et al. (2021b); **b** predicted values of ϕ_p for the 40 DC simulated on the digitised surfaces of sample K2 using the criterion by Ríos-Bayona et al. (2021b). The values in the boxes indicate the μ and σ of the predicted ϕ_p. **c** Comparison between the μ of predicted ϕ_p of samples K1 and K2 based on their simulated DC and predicted ϕ_p using their complete joint surfaces; **d** Comparison between the μ of predicted ϕ_p of samples K1 and K2 based on the 40 simulated DC and measured ϕ_p in the laboratory tests

ϕ_p for samples K1 and K2, based on their simulated DC, are respectively 1.3° and 1.8° higher than their predicted ϕ_p using their complete joint surfaces with dimensions of approximately 500×300 mm (see Fig. 14c).

A comparison between the respective μ of the predicted ϕ_p, based on the DC simulated on samples K1 and K2, and the ϕ_p measured in the laboratory tests, are presented in Fig. 14d. The μ of predicted ϕ_p for samples K1 and K2 based on their simulated DC are respectively 5.3° and 2.3° lower than their measured ϕ_p in the direct shear tests (see Fig. 14d).

8 Discussion

8.1 Prediction of Peak Shear Strength Based on Data from Simulated Drill Cores

As shown in Fig. 14c, the μ of predicted ϕ_p using the 40 DC simulated on samples K1 and K2, respectively, and the ϕ_p predicted using their entire joint surfaces, are in good agreement. The results presented in Fig. 14c validate the assumption made in Sect. 3.3 that the ϕ_p of samples K1 and K2 can be regarded as a mean value-driven process

of the contribution from each simulated DC on their digitised surfaces. Furthermore, the analysis performed on samples K1 and K2 show that the μ of predicted ϕ_p, based on the observed information of 3D surface roughness and joint aperture contained in the simulated DC, is in acceptable agreement with the measured ϕ_p in the laboratory (see Fig. 14d), even though the predicted ϕ_p is a few degrees lower than the measured ϕ_p.

The μ of the predicted ϕ_p of samples K1 and K2 based on the simulated 40 DC on their joint surfaces was respectively 5.3° and 2.3° lower than their measured ϕ_p in the direct shear tests (see Figs. 13b and 14c). A possible reason for the observed discrepancy between predicted and measured ϕ_p may be oscillation in the application of the shear displacement during the laboratory tests, which originated from a non-optimal control setting in the servo-hydraulic unit. These oscillations in the shear displacement during the direct shear tests induced small oscillations in the applied shear force. Consequently, the ϕ measured during the tests showed a variability that may have influenced the measured ϕ_p of samples K1 and K2. The plots of ϕ in Fig. 13b show the maximum local values registered during the direct shear tests. It was assumed that the observed maximum local values of ϕ originated from the maximum shear force applied by the servo-hydraulic unit in each oscillation. However, to investigate the uncertainty due to the oscillations in the applied shear displacement, the effect of using the mean local values of measured ϕ during the direct shear tests was studied. The measured ϕ_p of samples K1 and K2 using the mean local values of measured ϕ are 52.9° and 45.4°, respectively. These values of ϕ_p are respectively 4.2° and 4.3° lower than the values of ϕ_p shown in Table 3, and therefore cannot explain the observed discrepancy.

Another possible reason for the discrepancy between the respective predicted and measured ϕ_p of samples K1 and K2 is uncertainty in the aperture measurements derived from their digitised joint surfaces. The aperture measurements in Fig. 7 were obtained after superposing the digitised joint surfaces of samples K1 and K2 prior to application of the σ_n used during the direct shear tests (i.e., 1 MPa). However, under normal loading of samples K1 and K2, the average δ_n measured with the vertical LVDTs at a σ_n of 1 MPa was 0.27 and 0.23 mm, respectively (see Fig. 13a). The average δ_n registered with the 2D-DIC measurements in sample K1 at a σ_n of 1 MPa was 0.11 mm (see Fig. 13a). The main difference between the registered δ_n using vertical LVDTs and 2D-DIC measurements is that the latter measures δ_n directly at the joint plane. Thus, the influence of additional δ_n from both the specimen holders and encapsulating material due to their stiffness and the applied σ_n is removed. The observed values of δ_n at 1 MPa of σ_n may have reduced the aperture between the respective contact surfaces of samples K1 and K2. Furthermore, a smaller aperture between the contact surfaces

of the tested samples may also have influenced the values of a_{50} measured in each simulated DC on the respective digitised surfaces of samples K1 and K2. Lower values of a_{50} imply lower values of k, and higher values of both i_n and predicted ϕ_p with the criterion by Ríos-Bayona et al. (2021b) [see Eqs. (1) to (4) and Fig. 2]. A new calculation was performed to study the influence of the average δ_n registered in the consolidating normal loading tests on the respective μ of predicted ϕ_p of samples K1 and K2 based on the simulated DC. The distance in the vertical direction of all coordinate points in the upper and lower digitised surfaces of samples K1 and K2 was reduced by 0.27 and 0.23 mm, respectively, based on the registered δ_n with the LVDTs. The results of this calculation show that the μ of predicted ϕ_p of samples K1 and K2 using the observations from the 40 simulated DC increases to 54.4° and 48.7°, respectively. A third calculation was performed for sample K1 by reducing the vertical distance of all coordinate points by 0.11 mm, which was the average δ_n registered in the 2D-DIC measurements. If the aperture of the digitised surfaces of sample K1 is adjusted considering the 2D-DIC measurements, the μ of predicted ϕ_p is 52.6°. As expected, the μ of predicted ϕ_p for samples K1 and K2 based on the observations made in the simulated DC after adjusting the aperture of their joint surfaces is higher than the predicted values of ϕ_p shown in Fig. 14c. The observed discrepancy between predicted and measured ϕ_p when using the values of δ_n registered with the LVDTs is reduced from 5.3° to 2.7° and from 2.3° to 1.0° for samples K1 and K2, respectively. If the value from the 2D-DIC measurements is used for sample K1, the observed discrepancy between the μ of predicted ϕ_p and measured ϕ_p is reduced from 5.3° to 4.5°. These reduced discrepancies indicate that it is the measured value of a_{50} under the prevailing level of σ_n that should be used in the prediction of the ϕ_p, rather than the a_{50} obtained prior to the application of the σ_n during the direct shear tests.

Additionally, as introduced in Sect. 5.5, the minimum aperture, i.e., $\min\left(z_{i,j}^{\mathrm{upper}} - z_{i,j}^{\mathrm{lower}}\right)$, observed between the digitised joint surfaces in some of the simulated DC on samples K1 and K2, was larger than 0. This means that there were areas of samples K1 and K2 at large size not initially in contact during the direct shear tests in the laboratory. For instance, the DC with dimensions of 60×60 mm simulated on samples K1 and K2 had been assumed to have contact prior to testing in the laboratory if they had been obtained after subdividing the surfaces of samples K1 and K2 as suggested in Bandis et al. (1981) and Hencher et al. (1993). If this had been the case, the measured ϕ_p in the direct shear tests with the smaller specimens might have been the result of the mobilisation of a group of asperities which are not in contact in the actual joint surfaces of samples K1 and K2 at large size. Consequently, the measured ϕ_p obtained after
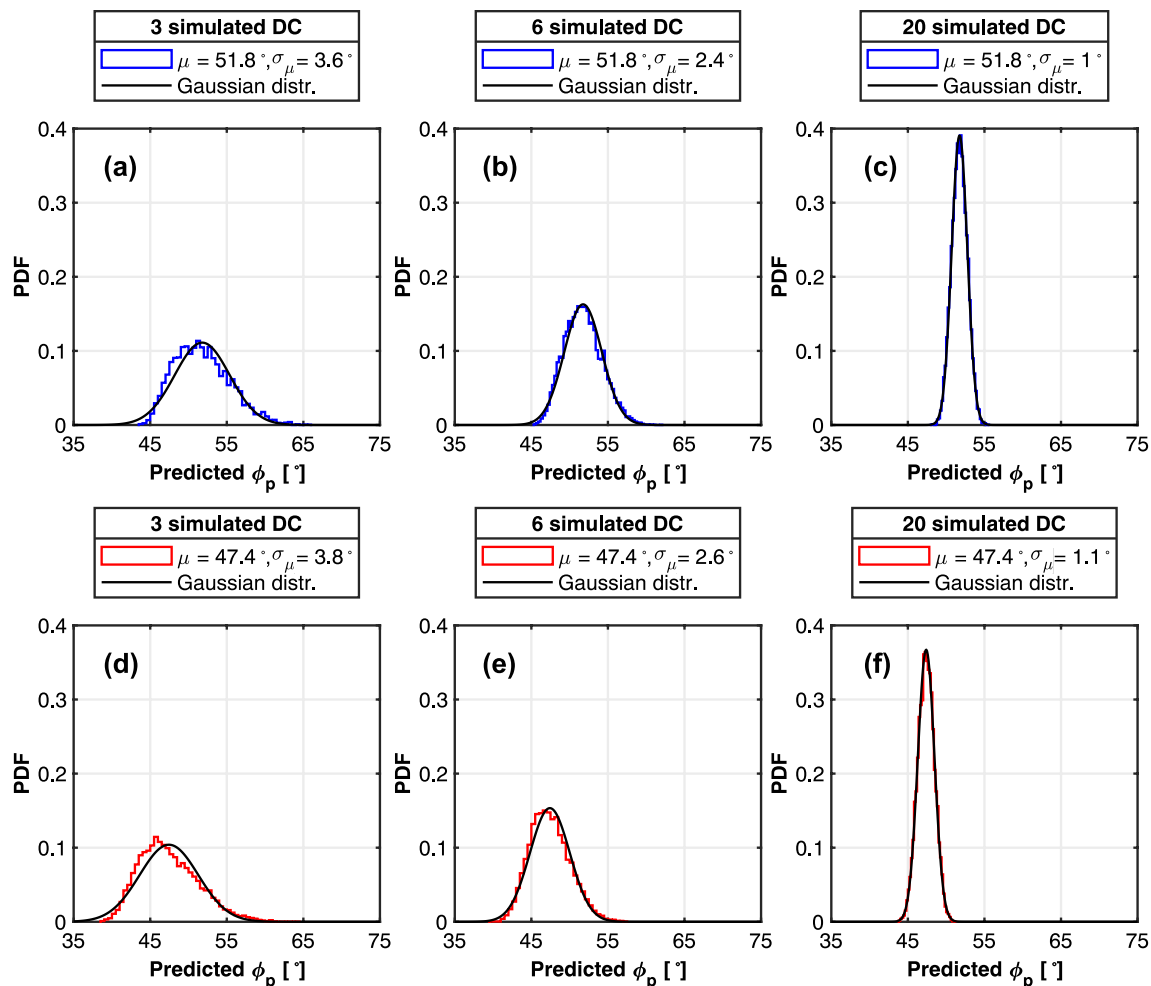
Fig. 15 Histograms of 10,000 Monte Carlo simulations with the predicted ϕ_p based on the 3D surface roughness and aperture of the simulated DC on sample K1: **a** using 3 simulated DC, **b** using 6 simulated DC and **c** using 20 simulated DC; and on sample K2: **d** using 3 simulated DC, **e** using 6 simulated DC, and **f** using 20 simulated DC. The continuous lines in each plot correspond to a Gaussian distribution with μ and σ_μ of the data set

shear testing the smaller specimens might not be a representative value in comparison with the measured ϕ_p on the large-size samples. As shown in Sect. 3 and Fig. 2, it is the aperture and surface roughness of a rock joint that governs the number, size and inclination of the active asperities in contact during the shearing process. However, the aperture between the contact surfaces is not commonly measured when investigating the influence of specimen size on the shear behaviour of rock joints (e.g., Pratt et al. 1974; Bandis et al. 1981; Yoshinaka et al. 1993; Ohnishi and Yoshinaka 1995; Giani et al. 1995; Castelli et al. 2001). Therefore, it is unclear if the reported scale effects in the literature were only caused by the size of the tested specimens. In the field, aperture measurements can be obtained directly in the borehole under the prevailing level of σ_n using a high-precision borehole camera system (Zou et al. 2021). The measuring

precision with the camera system used by Zou et al. (2021) was about 0.1 mm for borehole diameters up to 110 mm.

8.2 Influence of the Number of Drill Cores

In this study, the joint surfaces of samples K1 and K2 could be entirely observed and measured with laser scanning. In addition, the simulated DC covered the whole digitised surfaces of samples K1 and K2, respectively. This is usually not the case for large natural rock joints in the field. For instance, the uncertainty of the predicted ϕ_p of samples K1 and K2 is large when just one DC was randomly simulated (see Fig. 14a, b).

To increase this study's completeness, a Monte Carlo simulation was used to investigate the statistical uncertainty due to the number of drill cores (N_{DC}) used to predict the ϕ_p of samples K1 and K2. The predictions of ϕ_p were

performed by randomly selecting 3, 6, and 20 simulated DC on the digitised surfaces of samples K1 and K2, respectively. For each case, a total of 10,000 simulations were performed. The respective predicted ϕ_p of samples K1 and K2 in each simulation was calculated as the μ of the predicted ϕ_p of the randomly selected DC. The ϕ_p of each simulated DC on samples K1 and K2 is provided in Fig. 14a, b.

The histograms of 10,000 Monte Carlo simulations with the respective predicted ϕ_p of samples K1 and K2 using 3, 6, and 20 simulated DC are presented in Fig. 15. The results of the Monte Carlo simulations using 3, 6, and 20 DC simulated on sample K1 show that the μ of the predicted ϕ_p is 51.8° (see Fig. 15a–c). This value is similar to the μ of the predicted ϕ_p obtained with the 40 DC simulated on the whole surface of sample K1 (see Fig. 14a). The standard deviation of the mean values of predicted ϕ_p (σ_μ) of sample K1 using 3, 6, and 20 simulated DC are 3.6°, 2.4°, and 1.0°, respectively (see Fig. 15a, b, and c). The results of the Monte Carlo simulations using 3, 6, and 20 DC simulated on sample K2 show that the predicted ϕ_p has a μ of 47.4° (see Fig. 15d–f). This value of predicted ϕ_p is also similar to the ϕ_p predicted with the 40 DC simulated on sample K2 (see Fig. 14b). The values of σ_μ of the predicted ϕ_p using 3, 6, and 20 simulated DC on sample K2 are 3.8°, 2.6° and 1.1°, respectively (see Fig. 15d–f). The results of the Monte Carlo simulations with samples K1 and K2 clearly show that the statistical uncertainty in the prediction of their ϕ_p decreases with the increasing N_{DC} used in the analysis. Furthermore, the results presented in Fig. 15 suggest that the obtained distributions of predicted ϕ_p are close to Gaussian.

The results in Fig. 15 show that the σ_μ is large if only a few samples are considered. In previous studies, the

influence of σ_μ has usually not been properly accounted for when comparing the results from direct shear tests at different sizes (e.g., Bandis et al. 1981; Kutter and Otto 1990; Yoshinaka et al. 1993; Ohnishi and Yoshinaka 1995; Castelli et al. 2001). This may partly explain some of the conflicting results regarding the scale effect reported in the literature, in addition to the influence from surface aperture previously discussed in Sect. 8.1.

In statistical terms, the values of σ_μ obtained in the Monte Carlo simulations using different N_{DC}, as shown in Fig. 15, can be estimated using the equation that describes the standard deviation of the mean value of a population (Curran-Everett et al. 1998; Altman and Bland 2005). This can be expressed as

$$\sigma_\mu = \frac{\sigma_{DC}}{\sqrt{N_{DC}}}, \tag{11}$$

where σ_{DC} is the standard deviation of the ϕ_p predicted with the 40 DC simulated on samples K1 and K2, respectively (see Fig. 14a, b)

A sensitivity analysis with the influence of N_{DC} on the value of σ_μ using Eq. (11), when predicting the ϕ_p of samples K1 and K2, and its comparison with the values of σ_μ obtained in the Monte Carlo simulations, is illustrated in Fig. 16. The reduction of the value of σ_μ using Eq. (11) with increasing N_{DC}, used to predict the ϕ_p of samples K1 and K2, is in good agreement with the σ_μ of the μ of predicted ϕ_p in the Monte Carlo simulations (see Fig. 15).

8.3 Prediction of Peak Shear Strength in the Field

The novelty of this paper lies in the use of data obtained from drill cores to predict the ϕ_p of large-size natural, unfilled rock joints. In this study, the digitised joint surfaces of two rock joint samples of coarse-grained granite are used to predict their ϕ_p based on observations of the 3D roughness and aperture obtained from simulated drill cores. The respective ϕ_p values of the tested samples are predicted based on the theory presented in Sect. 3.3 and using the peak shear strength criterion by Ríos-Bayona et al. (2021b) in Sect. 3.1. The results obtained from both the laboratory experiments on the analysed samples, and the prediction of their ϕ_p using the simulated drill cores, indicate that aperture measurements should be directly surveyed in the borehole at the actual level of σ_n. This is of importance to realistically measure the actual aperture of large natural, unfilled rock joints in the field under conditions of difficult access, such as the rock foundation under a concrete dam.

The results of the Monte Carlo simulations show that the statistical uncertainty of the predicted ϕ_p of samples K1 and K2 decreases with increasing number of drill cores used in the analysis. Furthermore, the results presented in
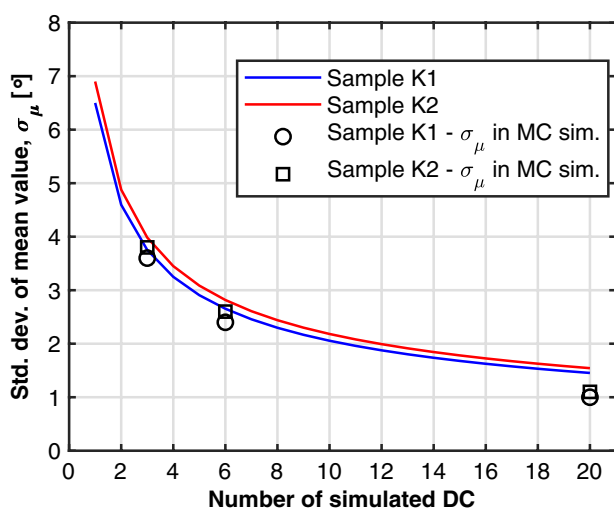

Fig. 16 Influence of N_{DC} on the value of σ_μ using Eq. (11) when predicting the ϕ_p of samples K1 and K2, and its comparison with the values of σ_μ obtained in the Monte Carlo simulations

this study show that the relationship between the statistical uncertainty of the predicted ϕ_p and the number of drill cores used in the prediction can be quantified, as shown in Fig. 16. For instance, the number of drill cores and its associated level of uncertainty on the prediction of the peak shear strength is of significant importance when performing sliding stability analysis in the rock foundation under a concrete dam applying a reliability-based methodology.

However, some issues remain concerning the suggested approach that require further attention before it is applied in the field. For example, it is worth to discuss the minimum required distance between the drill cores. In the analysis performed in this paper, all simulated DC on each sample originate from the same joint surface. That all samples at small size originate from the same rock joint is also a pre-requisite for the theory in Sect. 3.3 to be valid. However, it may be difficult to identify a single specific rock joint, since other rock joints may be located nearby. If the rock joint under study is very distinctive compared to other rock joints in the rock mass, it can be easy to identify. Under such condition, three boreholes may be sufficient to identify the rock joint's orientation, even though the statistical uncertainty of the predicted ϕ_p in that case will be large (see Fig. 15a, d). On the other hand, in a more fractured rock mass, a shorter distance between the drill cores may most likely be required to be able to follow the joint in the rock mass. Another factor that influences the required distance between drill cores is their diameter. When characterising surface roughness of rock joints in the field, it is well known that the variation of asperity inclination increases with a decrease in the asperity base length (e.g., Sfondrini and Sterlacchini 1996). Therefore, the uncertainty in the determination of a rock joint's strike and dip values increases with small diameters of the drill cores, especially for rough joint surfaces. It is therefore important to have a good understanding of the geological mechanisms that created the rock joint under study and its characteristics. It is also important that the core samples are correctly oriented to identify their potential shear direction in 3D. If a correct orientation is not obtained, roughness anisotropy associated to different shear directions should be considered. The evaluation of roughness anisotropy using three-dimensional surface measurements can be done by applying the methodology described by Tatone and Grasselli (2009). The parameters associated with the 3D surface roughness of the rock joint samples analysed in this study (A_0, θ^*_{max}, C and H) were calculated for a known shear direction and a defined shear plane. Additionally, the criterion by Ríos-Bayona et al. (2021b) was developed to predict the ϕ_p of natural, unfilled rock joints. That no infilling material is present needs to be verified before the presented methodology can be applied to predict the peak shear strength with the criterion by Ríos-Bayona et al. (2021b). The presence

of infilling material may be investigated using a triple tube core-drilling technique.

A limitation with the current study is that the presented methodology has only been applied to two rock joint samples of granite tested with low normal stress to joint wall compressive strength ratios of approximately 0.01. Further studies with samples of both same and other rock types, and under higher levels of applied σ_n, are required to further investigate the ability of this methodology to predict the ϕ_p of large natural, unfilled rock joints in the field.

9 Conclusions

In this paper, we present a novel methodology that predicts the peak shear strength of two large natural, unfilled rock joint samples. The methodology uses information of surface roughness and aperture obtained from small-size samples simulated on the joint surfaces of the large samples. Based on the performed analysis and experiments in the laboratory on the two samples, it can be concluded that the simulated drill cores contain the necessary information to predict their peak shear strength with acceptable results under the conditions tested in this study. However, the application of this methodology both under different conditions and in the field remains to be tested in future research.

The obtained results show that a sufficient number of drill cores needs to be used to reduce the statistical uncertainty of the predicted peak shear strength of the tested large-size samples. Furthermore, the performed analyses show that the rock joint aperture needs to be accounted for and measured directly in the borehole to accurately predict the peak shear strength of the large-size samples. The main benefit of this approach is that it may enable prediction of the peak shear strength of large natural, unfilled rock joints under conditions of difficult access, such as the rock foundation under an existing concrete dam.

A limitation with the proposed methodology is its applicability only for natural, unfilled rock joints. The absence of any infilling material between the joint surfaces of large natural rock joints must be established before applying the methodology presented in this study. Infilling material may be identified in the field using a triple tube core-drilling technique. Furthermore, the samples analysed in this study consisted of granite and were tested with low normal stress to joint wall compressive strength ratios of approximately 0.01. It is therefore recommended that further studies be conducted on different rock types at higher levels of normal stress to joint wall compressive strength ratios to assess the applicability of the presented methodology under such conditions.

Declarations

Conflict of interest The authors declare that they have no conflicts of interest.

References

Alejano LR, González J, Muralha J (2012) Comparison of different techniques of tilt testing and basic friction angle variability assessment. Rock Mech Rock Eng 45:1023–1035. https://doi.org/10.1007/s00603-012-0265-7

Alejano LR et al (2018) ISRM suggested method for determining the basic friction angle of planar rock surfaces by means of tilt tests. Rock Mech Rock Eng 51:3853–3859. https://doi.org/10.1007/s00603-018-1627-6

Altman DG, Bland JM (2005) Standard deviations and standard errors. BMJ 331:903. https://doi.org/10.1136/bmj.331.7521.903

Aydin A (2008) ISRM suggested method for determination of the schmidt hammer rebound hardness: revised version. In: Ulusay R (ed) The ISRM suggested methods for rock characterization, testing and monitoring: 2007–2014. Springer, Cham

Bandis S, Lumsden A, Barton N (1981) Experimental studies of scale effects on the shear behaviour of rock joints. Int J Rock Mech Min Sci Geomech Abstr 18:1–21. https://doi.org/10.1016/0148-9062(81)90262-X

Bandis S (1980) Experimental studies of scale effects on shear strength, and deformation of rock joints. Doctoral Thesis, University of Leeds

Barla G, Robotti F, Vai L (2011) Revisiting large size direct shear testing of rock mass foundations. In: Pina C, Portela E, Gomes J (eds) 6th International Conference on Dam Engineering, Lisbon, Portugal. LNEC, Lisbon

Barton N, Bandis S (1982) Effects of block size on the shear behavior of jointed rock. In: The 23rd US symposium on rock mechanics (USRMS), 1982. American Rock Mechanics Association

Barton N, Choubey V (1977) The shear strength of rock joints in theory and practice. Rock Mech 10:1–54. https://doi.org/10.1007/BF01261801

Bowden FP, Tabor D (1950a) The friction and lubrication of solids, vol 1. Oxford University Press, London

Bowden FP, Tabor D (1950b) The friction and lubrication of solids, vol 2. Oxford University Press, London

Brown SR (1987) A note on the description of surface roughness using fractal dimension. Geophys Res Lett 14:1095–1098. https://doi.org/10.1029/GL014i011p01095

Buzzi O, Casagrande D (2018) A step towards the end of the scale effect conundrum when predicting the shear strength of large in situ discontinuities. Int J Rock Mech Min Sci 105:210–219. https://doi.org/10.1016/j.ijrmms.2018.01.027

Casagrande D, Buzzi O, Giacomini A, Lambert C, Fenton G (2018) A new stochastic approach to predict peak and residual shear strength of natural rock discontinuities. Rock Mech Rock Eng 51:69–99. https://doi.org/10.1007/s00603-017-1302-3

Castelli M, Re F, Scavia C, Zaninetti A (2001) Experimental evaluation of scale effects on the mechanical behavior of rock joints. In: Proceedings of International Eurock Symposium. Espoo, Finland. p 205–210

Curran-Everett D, Taylor S, Kafadar K (1998) Fundamental concepts in statistics: elucidation and illustration. J Appl Physiol 85:775–786. https://doi.org/10.1152/jappl.1998.85.3.775

Du W, Ban L, Qi C (2021) Reply to the discussion by Yingchun Li on "A Peak Dilation Angle Model Considering the Real Contact Area for Rock Joints." Rock Mech Rock Eng. https://doi.org/10.1007/s00603-021-02581-1

Giani GP, Ferrero AM, Passarella G, Reinaudo L (1995) Scale effect evaluation on natural discontinuity shear strength. In: Myer LR, Cook NGW, Goodman RE, Tsang CF (eds) Fractured and Jointed Rock Masses. Balkema, Rotterdam, pp 447–452

Grasselli G, Egger P (2003) Constitutive law for the shear strength of rock joints based on three-dimensional surface parameters. Int J Rock Mech Min Sci 40:25–40. https://doi.org/10.1016/S1365-1609(02)00101-6

Grasselli G, Wirth J, Egger P (2002) Quantitative three-dimensional description of a rough surface and parameter evolution with shearing. Int J Rock Mech Min Sci 39:789–800. https://doi.org/10.1016/S1365-1609(02)00070-9

Grasselli G (2001) Shear strength of rock joints based on quantified surface description. Doctoral Thesis, Lausanne, EPFL

Hencher SR, Richards LR (2015) Assessing the shear strength of rock discontinuities at laboratory and field scales. Rock Mech Rock Eng 48:883–905. https://doi.org/10.1007/s00603-014-0633-6

Hencher S, Toy J, Lumsden A (1993) Scale dependent shear strength of rock joints. In: Pinto Da Cunha A (ed) Scale effects in rock masses, vol 93. CRC Press, London, pp 233–240

Huang M, Hong C, Du S, Luo Z (2020a) Experimental technology for the shear strength of the series-scale rock joint model. Rock Mech Rock Eng 53:5677–5695. https://doi.org/10.1007/s00603-020-02241-w

Huang M, Hong C, Ma C, Luo Z, Du S, Yang F (2020b) A new representative sampling method for series size rock joint surfaces. Sci Rep 10:9129. https://doi.org/10.1038/s41598-020-66047-0

Jacobsson L, Ivars DM, Kasani HA, Johansson F, Lam T (2021) Experimental program on mechanical properties of large rock fractures. IOP Conf Ser: Earth Environ Sci 833:012015. https://doi.org/10.1088/1755-1315/833/1/012015

Johansson F (2016) Influence of scale and matedness on the peak shear strength of fresh, unweathered rock joints. Int J Rock Mech Min Sci 82:36–47. https://doi.org/10.1016/j.ijrmms.2015.11.010

Johansson F, Stille H (2014) A conceptual model for the peak shear strength of fresh and unweathered rock joints. Int J Rock Mech Min Sci 69:31–38. https://doi.org/10.1016/j.ijrmms.2014.03.005

Kutter H, Otto F (1990) Influence of parallel and cross joints on shear behaviour of rock discontinuities. In: Proceedings of the First International Workshop on Scale Effects in Rock Masses, Loen, 7–8 June 1990. p 243–250

Lanaro F (2000) A random field model for surface roughness and aperture of rock fractures. Int J Rock Mech Min Sci 37:1195–1210. https://doi.org/10.1016/S1365-1609(00)00052-6

Larsson J (2021) Experimental investigation of the system normal stiffness of a 5 MN direct shear test setup and the compensation of it in CNS direct shear tests. IOP Conf Ser: Earth Environ Sci 833:012011. https://doi.org/10.1088/1755-1315/833/1/012011

Li Y (2021) Discussion on "A Peak Dilation Angle Model Considering the Real Contact Area for Rock Joints" Liren Ban, Weisheng Du and Chengzhi Qi, Rock Mech Rock Eng, DOI: 10.1007/s00603-020-02193-1. Rock Mech Rock Eng. https://doi.org/10.1007/s00603-021-02440-z

Malinverno A (1990) A simple method to estimate the fractal dimension of a self-affine series. Geophys Res Lett 17:1953–1956. https://doi.org/10.1029/GL017i011p01953

Mandelbrot BB (1985) Self-affine fractals and fractal dimension. Phys Scr 32:257

Muralha J, Pinto Da Cunha A (1990) About LNEC experience on scale effects in the mechanical behaviour of joints. In: Pinto Da Cunha A (ed) Scale effect in rock masses. Balkema, Rotterdam

Muralha J, Grasselli G, Tatone B, Blümel M, Chryssanthakis P, Yujing J (2014) ISRM suggested method for laboratory determination of the shear strength of rock joints: revised version. Rock Mech Rock Eng 47:291–302. https://doi.org/10.1007/s00603-013-0519-z

Myers N (1962) Characterization of surface roughness. Wear 5:182–189. https://doi.org/10.1016/0043-1648(62)90002-9

Odling NE (1994) Natural fracture profiles, fractal dimension and joint roughness coefficients. Rock Mech Rock Eng 27:135–153. https://doi.org/10.1007/BF01020307

Ohnishi Y, Yoshinaka R (1995) Laboratory investigation of scale effect in mechanical behavior of rock joint. In: Myer C, Goodman T (eds) Fractured and jointed rock masses. Balkema, Rotterdam, pp 465–470

Pratt H, Black A, Brace W (1974) Friction and deformation of jointed quartz diorite. In: Proc. 3rd ISRM Congress, Denver, p 306–310

Renard F, Voisin C, Marsan D, Schmittbuhl J (2006) High resolution 3D laser scanner measurements of a strike-slip fault quantify its morphological anisotropy at all scales. Geophys Res Lett. https://doi.org/10.1029/2005GL025038

Renaud S, Bouaanani N, Miquel B (2021) Experimental, analytical, and finite element assessment of the shear strength of concrete-rock interfaces at different scales. Int J Numer Anal Meth Geomech 45:1238–1259. https://doi.org/10.1002/nag.3195

Ríos-Bayona F, Andersson E, Johansson F, Mas Ivars D (2021a) The importance of accounting for matedness when predicting the peak shear strength of rock joints. IOP Conf Ser: Earth Environ Sci 833:012017. https://doi.org/10.1088/1755-1315/833/1/012017

Ríos-Bayona F, Johansson F, Mas-Ivars D (2021b) Prediction of peak shear strength of natural, unfilled rock joints accounting for matedness based on measured aperture. Rock Mech Rock Eng 54:1533–1550. https://doi.org/10.1007/s00603-020-02340-8

Sfondrini G, Sterlacchini S (1996) Influence of joint roughness on discontinuity shear strength. In: Proc. Safety and Environmental Issues on Rock Engineering. Eurock 96. p 135–143

Stigsson M, Mas Ivars D (2019) A novel conceptual approach to objectively determine JRC using fractal dimension and asperity distribution of mapped fracture traces. Rock Mech Rock Eng. https://doi.org/10.1007/s00603-018-1651-6

Tatone BS, Grasselli G (2009) A method to evaluate the three-dimensional roughness of fracture surfaces in brittle geomaterials. Rev Sci Instrum 80:125110. https://doi.org/10.1063/1.3266964

Yong R, Qin J-B, Huang M, Du S-G, Liu J, Hu G-J (2019) An innovative sampling method for determining the scale effect of rock joints. Rock Mech Rock Eng 52:935–946. https://doi.org/10.1007/s00603-018-1627-6

Yoshinaka R, Yoshida J, Arai H, Arisaka S (1993) Scale effects on shear strength and deformability of rock joints. In: Pinto Da Cunha A (ed) Scale Effects in Rock Masses 93. CRC Press, London, pp 143–149

Zhao J (1997a) Joint surface matching and shear strength part A: joint matching coefficient (JMC). Int J Rock Mech Min Sci 34:173–178. https://doi.org/10.1016/S0148-9062(96)00062-9

Zhao J (1997b) Joint surface matching and shear strength part B: JRC-JMC shear strength criterion. Int J Rock Mech Min Sci 34:179–185. https://doi.org/10.1016/S0148-9062(96)00063-0

Zou X, Song H, Wang C (2021) A high-precision digital panoramic borehole camera system for the precise analysis of in situ rock structures. Rock Mech Rock Eng. https://doi.org/10.1080/17486025.2014.884728

Publisher's Note Springer Nature remains neutral with regard to jurisdictional claims in published maps and institutional affiliations.